Understanding bias in the evaporative damping of El Niño–Southern Oscillation events in CMIP5 models

Article

Published Version

It is advisable to refer to the publisher's version if you intend to cite from the work. See Guidance on citing.

Publisher: American Meteorological Society

www.reading.ac.uk/centaur

CentAUR

Central Archive at the University of Reading

Reading's research outputs online

Understanding Bias in the Evaporative Damping of El Niño–Southern Oscillation Events in CMIP5 Models

SAMANTHA FERRETT AND MATTHEW COLLINS

College of Engineering, Mathematics and Physical Sciences, University of Exeter, Exeter, United Kingdom

HONG-LI REN

Laboratory for Climate Studies, National Climate Center, China Meteorological Administration, Beijing, and Department of Atmospheric Science, School of Environmental Studies, China University of Geoscience, Wuhan, and CMA–Nanjing University Joint Laboratory for Climate Prediction Studies, School of Atmospheric Sciences, Nanjing University, Nanjing, China

ABSTRACT

This study examines the extent of the Pacific double–intertropical convergence zone (ITCZ) bias in an ensemble of CMIP5 coupled general circulation models and the relationship between this common bias and equatorial Pacific evaporative heat flux feedbacks involved in El Niño–Southern Oscillation (ENSO). A feedback decomposition method, based on the latent heat flux bulk formula, is implemented to enable identification of underlying causes of feedback bias and diversity from dynamical and thermodynamical processes. The magnitude of mean precipitation south of the equator in the east Pacific (an indicator of the extent of the double-ITCZ bias in a model) is linked to the mean meridional surface wind speed and direction in the region and is consequently linked to diversity in the strength of the wind speed response during the ENSO cycle. The ENSO latent heat flux damping is weak in almost all models and shows a relatively large range in strength in the CMIP5 ensemble. While both humidity gradient and wind speed feedbacks are important drivers of the damping, the wind speed feedback is an underlying cause of the overall damping bias for many models and is ultimately more dominant in driving interensemble variation. Feedback biases can also persist in atmosphere-only (AMIP) runs, suggesting that the atmosphere model plays an important role in latent heat flux damping and double-ITCZ bias and variation. Improvements to coupled model simulation of both mean precipitation and ENSO may be accelerated by focusing on the atmosphere component.

1. Introduction

The mean tropical Pacific climate is characterized by a zonal SST gradient along the equator as well as warmer temperatures, precipitation, and atmospheric ascent in the west equatorial Pacific and regions off the equator. Zonal and meridional atmospheric circulations (i.e., the Walker and Hadley circulations) reinforce this climate. A band of intense precipitation, the intertropical convergence zone (ITCZ), lies to the north of the equator, and a similar region of intense precipitation, named the South Pacific convergence zone (SPCZ), lies to the south of the equator. The precipitation and atmospheric ascent in the SPCZ typically do not extend as far east as in the more prominent ITCZ, resulting in a meridional asymmetry in the mean tropical Pacific climate. This mean state provides the background for interannual variability such as El Niño–Southern Oscillation (ENSO), a dominant mode of variability that has a large impact on weather events worldwide.

Coupled general circulation models (CGCMs) used for climate projections suffer from persistent mean-state equatorial Pacific climate biases (Guilyardi 2006; Lin 2007; Brown et al. 2013; Bellenger et al. 2014; Zhang et al. 2015), resulting in uncertainty in those projections. In particular, CGCMs show a cooler region in the east Pacific (cold tongue) that tends to extend too far west compared with observations. They also show bias in the meridional asymmetry of the mean tropical Pacific climate, exhibiting a more zonally extended region of precipitation in the southwest Pacific, a bias known as the "double-ITCZ bias." In models featuring this bias, precipitation off the equator in the Pacific is often too strong (Mechoso et al. 1995; Lin 2007; de Szoeke and

Corresponding author: Samantha Ferrett, s.ferrett@exeter.ac.uk

Xie 2008; Li and Xie 2014; Zhang et al. 2015). It is suggested that the double-ITCZ bias mainly lies in the atmospheric models rather than the ocean component (Schneider 2002; Li and Xie 2012; Vannière et al. 2013), although the ocean model and the coupling to the atmosphere may also play an important role in maintaining the cold tongue bias via the zonal wind–SST (Bjerknes) feedback (Li and Xie 2012, 2014). Attempts at eliminating the bias have involved modifying the convection parameterization scheme and adjusting surface winds (Hess et al. 1993; Frey et al. 1997; Luo et al. 2005; Zhang and Wang 2006; Song and Zhang 2009; Zhang and Song 2010; Chikira and Sugiyama 2010). However, a recent study by Zhang et al. (2015) finds that the double-ITCZ bias still persists in more recent coupled climate models (e.g., CMIP5).

Ocean–atmosphere feedbacks driving ENSO-related variability are also often quite different from observational estimates, as are other ENSO characteristics such as amplitude and period (AchutaRao and Sperber 2006; Guilyardi 2006; Zhang and Jin 2012; Zhang et al. 2013; Bellenger et al. 2014; Zhang and Sun 2014). This is often referred to as model "diversity." The mean equatorial Pacific climate is known to play an important role in the feedbacks driving ENSO-related variability (An and Jin 2000; Guilyardi 2006; Fedorov and Philander 2001; Santoso et al. 2011; Kim et al. 2014b). Jin et al. (2006) introduced a way to quantify these ocean–atmosphere feedbacks, known as the Bjerknes (BJ) stability index, by using various linear approximations. This allowed links to be established between ENSO feedbacks and the tropical Pacific mean climate. For example, Kim et al. (2014b) link ENSO feedback diversity to mean climate diversity in multimodel ensembles. In particular, they find that the strength of ENSO ocean current feedbacks can be linked to mean zonal surface wind stress and ocean temperature.

The modulation of east equatorial Pacific SST by anomalous heat flux, known as thermodynamic damping, is another dominant ENSO feedback and an important source of ENSO diversity in coupled climate models (Jin et al. 2006; Kim and Jin 2011; Kim et al. 2014b; Lloyd et al. 2009). The strength of this feedback in both multimodel and perturbed physics ensembles has also been found to be linked to mean climate, namely mean SST (Kim et al. 2014b) and mean precipitation (Ferrett and Collins 2016). The underlying mechanisms of these relationships in coupled climate models have yet to be studied in detail.

Latent heat flux (LHF) is a dominant contributor to the thermodynamic damping of ENSO sea surface temperature anomalies (SSTAs), alongside shortwave radiation. The damping of east equatorial Pacific SSTAs by anomalous evaporation, the latent heat flux damping (Wallace 1992), has been diversely represented in previous generations of coupled climate models and the strength of this feedback is often not fully captured (Lloyd et al. 2009, 2011; Lin 2007). While LHF damping has been slightly improved in the current generation of coupled climate models, CMIP5 (Taylor et al. 2012), biases still persist in this key ENSO feedback (Bellenger et al. 2014). ENSO feedback discrepancies can cause uncertainty in ENSO projections. For example, Kim et al. (2014a) found that multimodel projections of ENSO feedbacks became more robust when a subset of CMIP5 models with the most accurate ENSO feedbacks was studied.

Latent heat flux can be estimated by a bulk formula (Fairall et al. 1996, 2003) expressing LHF in terms of near-surface specific humidity difference and surface wind speed. An increase in the near-surface humidity gradient increases evaporation, as does an increase in surface wind speed. However, the relative contribution these components have to total latent heat flux can vary based on a number of factors, and the ways in which both the dynamic (wind speed) and thermodynamic (humidity gradient) components interact with each other mean that determining the underlying causes of latent heat diversity can be complex.

Lloyd et al. (2011) examine east Pacific LHF damping (the strength of latent heat flux response to SSTAs) in a number of coupled models from phase 3 of the Coupled Model Intercomparison Project (CMIP3) and suggest that biases in LHF damping strength are primarily caused by insufficient responses of the near-surface humidity gradient to east Pacific SSTAs. In particular, they note weak responses of near-surface specific humidity to SSTAs. Lloyd et al. (2011) also suggest that biases in the dynamical response (surface wind speed feedback) contribute to the LHF damping bias in some models. Lin (2007) found that the mean equatorial Pacific climate in coupled climate models can be linked to LHF damping diversity (i.e., linking the persistent double-ITCZ bias to LHF damping via an excessive sensitivity of near-surface humidity to SST). Xie and Philander (1994) also suggest that the wind speed feedback is important in maintaining the position of the ITCZ via the impact of wind speed on latent heat flux (WES feedback), implying a link between mean equatorial Pacific climate and LHF feedback. A number of studies have also suggested links between various other ocean–atmosphere feedbacks and the mean equatorial Pacific asymmetry. For example, the stratus–SST feedback or the shortwave heat flux feedback (Li and Philander 1996; Philander et al. 1996) and meridional wind–upwelling–SST feedback (Mitchell and Wallace 1992; Chang and Philander 1994).

Under the assumption of the bulk formula, latent heat flux is the product of humidity difference and wind

TABLE 1. The reanalyses and CMIP5 models (Taylor et al. 2012) used in this study. Simulations of the historical experiment over the time period 1950–99 are used throughout. Observations and reanalysis datasets cover 1985–2009. Asterisks indicate when CMIP5 models are compared to atmosphere-only model (AMIP) runs. (Expansions of acronyms are available online at http://www.ametsoc.org/PubsAcronymList.)

No.	Name	Modeling center
0a	OAFlux and GPCP (precipitation)	
0b	NCEP-2	
0c	ERA-Interim	
1	BCC_CSM1.1(m)	Beijing Climate Center, China Meteorological Administration
2	BNU-ESM*	College of Global Change and Earth System Science, Beijing Normal University
3	CanESM2	Canadian Centre for Climate Modelling and Analysis
4	CSIRO Mk3.6.0*	Commonwealth Scientific and Industrial Research Organisation in collaboration with Queensland Climate Change Centre of Excellence
5a	GFDL CM3*	NOAA/Geophysical Fluid Dynamics Laboratory
5b	GFDL-ESM2M	
6	HadGEM2-ES	Met Office Hadley Centre (additional realizations contributed by Instituto Nacional de Pesquisas Espaciais)
7a	IPSL-CM5A-LR*	L'Institut Pierre-Simon Laplace
7b	IPSL-CM5A-MR*	
7c	IPSL-CM5B-LR*	
8a	MIROC4h	Atmosphere and Ocean Research Institute (The University of Tokyo), National Institute for Environmental Studies, and Japan Agency for Marine-Earth Science and Technology
8b	MIROC5*	
9	MRI-ESM1	Meteorological Research Institute

speed. This means that studies such as those of Lin (2007) and Lloyd et al. (2011) that examine responses of near-surface humidity difference or wind speed to SSTAs separately as underlying causes of LHF damping bias may be missing important parts of the picture arising from the nonlinear interaction between the two components. Lloyd et al. (2011) implement a decomposition of LHF that accounts for this (e.g., Zhang and McPhaden 1995; Alexander and Scott 1997) and allows the separation of nonlinear and linear components of LHF. However, they examine the behavior of LHF during a single observed El Niño, finding that the anomalous humidity difference component dominates LHF variability, rather than assess interensemble diversity of LHF damping using such a decomposition. As such, there is scope for implementation of this type of east Pacific LHF damping decomposition over a set time period in current coupled climate models, therefore capturing multiple ENSO events. This would help to identify underlying causes of LHF damping bias and the relationship they have with equatorial Pacific mean climate diversity.

Here, we aim to quantify the relationship between the prominent double-ITCZ bias and atmospheric ENSO feedbacks. This study primarily focuses on the relationship between this bias and latent heat flux feedback via wind speed and near-surface humidity gradient feedbacks in the most recent generation of CGCMS, CMIP5. To do this we implement feedback decomposition to identify underlying mechanisms of these

links, with the aim of highlighting metrics that allow quantification of these relationships and to help prioritize the development of future climate models to improve our confidence in ENSO projections.

The layout of the study is as follows: section 2 introduces the CMIP5 models and reanalysis datasets used, and section 3 outlines the methodology, including latent heat and wind speed feedback decompositions. Sections 4 and 5 go on to describe the results of mean Pacific climate analysis and the relationship between mean atmospheric circulation and ENSO atmospheric feedbacks. A summary of the results is given in section 6 along with suggestions for areas of future research.

2. Data

a. CMIP5 and AMIP

This study uses historical experiments over the time period 1950–99 for 13 coupled climate models from the World Climate Research Programme (WCRP) CMIP5 multimodel ensemble (Taylor et al. 2012). Details of the models used are given in Table 1 and were chosen based on availability of daily mean fields of the required variables. Seasonal anomalies used in the latent heat flux decomposition (temperature, humidity, and surface wind speed fields) are constructed from daily data as this improves the accuracy of the decomposition detailed in section 3. Results from CMIP5 models are also

compared to atmosphere-only model (AMIP) runs for seven of the coupled models (indicated in Table 1 by an asterisk by the model name). AMIP analysis is over the time period 1979–2008 and uses monthly mean fields to calculate latent heat flux for decomposition. Monthly fields are used for the calculation of time means of temperature and precipitation.

b. Observations and reanalyses

Four sets of reanalysis/analysis data are used in comparison to the models. These are ECMWF ERA-Interim (Dee et al. 2011), objectively analyzed air–sea heat fluxes (OAFlux; Yu and Weller 2007), NCEP–DOE 2 (Kanamitsu et al. 2002), and the Global Precipitation Climatology Project version 2.3 combined precipitation dataset (GPCP; Adler et al. 2003). Daily mean data are used for the first three datasets and monthly means are used for GPCP. All reanalysis datasets are used for 1985–2009. Shortwave and longwave radiation for OAFlux are provided by ISCCP (Schiffer and Rossow 1983).

3. Methods

a. Latent heat damping decomposition

The analysis of downward latent heat flux used here is based on the following bulk formula:

$$Q_{LH} = -c_L L_E \rho U \Delta q = -c_L L_E \rho (\overline{U} + U')(\overline{\Delta q} + \Delta q'), \quad (1)$$

where Q_{LH} is latent heat flux, U is the wind speed, and $\Delta q = q_s - q_a$ is the near-surface specific humidity difference, where surface specific humidity q_s is calculated using sea surface temperature (Ambaum 2010) and the Goff–Gratch equation for saturation water vapor pressure (Goff and Gratch 1946; Goff 1957) and q_a is the specific humidity at 10 m. Also, c_L is the turbulent moisture exchange coefficient, L_E is the latent heat of evaporation, and ρ is the air density at the surface; x' indicates the seasonal anomaly of x averaged over the Niño-3 area (5°S–5°N, 150°–90°W) and an overbar represents the time-mean Niño-3 area average. Equation (1) can be decomposed (e.g., Zhang and McPhaden 1995) to find the anomalous component so that

$$Q'_{LH} = -c_L L_E \rho (\overline{U} \Delta q' + \overline{\Delta q} U'). \quad (2)$$

This is obtained under the assumption that $\Delta q' U'$ is negligible.

Niño-3 latent heat flux damping, α_{LH} (e.g., Lloyd et al. 2009), can be found such that

$$Q'_{LH} = \alpha_{LH} T' \quad (3)$$

by linear regression of Niño-3 averaged latent heat flux seasonal anomalies on Niño-3 averaged SST T seasonal anomalies. Seasonal anomalies are detrended prior to linear regression. Monthly values of q_a, q_s, Q_{LH}, U, and T are all calculated from daily fields. From Eqs. (2) and (3) it is then possible to obtain the LHF damping components:

$$-c_L L_E \rho \overline{U} \Delta q' = \alpha_{\Delta q} T' \quad \text{and} \quad (4)$$

$$-c_L L_E \rho \overline{\Delta q} U' = \alpha_U T', \quad (5)$$

where

$$\alpha_{LH} = \alpha_{\Delta q} + \alpha_U. \quad (6)$$

This finds a thermodynamic component of LHF damping arising primarily from anomalous near-surface humidity difference ($\alpha_{\Delta q}$) and a dynamic component driven by anomalous surface wind speed (α_U). For ease, these components will be referred to as the humidity gradient and wind speed (WS) feedbacks throughout. A negative value for these feedbacks means humidity gradient or wind speed anomalies are contributing to increased evaporation in response to a positive SSTA, hence damping the SST anomaly. Conversely, a positive value corresponds to a positive feedback on SST.

b. Wind speed decomposition and precipitation response symmetry

Wind speed is calculated for each grid box using zonal and meridional wind speed fields so that

$$U^2 = u^2 + v^2, \quad (7)$$

where U is wind speed, u is zonal wind speed, and v is meridional wind speed. We make the assumption that seasonal wind speed anomalies, U', can be expressed as a linear combination of zonal and meridional wind speed anomalies, $|u|'$ and $|v|'$:

$$U' \approx \beta_u |u|' + \beta_v |v|', \quad (8)$$

for some constants β_u and β_v, obtained using linear regression. This is found to be a valid approximation (99% significance by a Student's t test) for all the models used in this study.

Combining Eq. (8) with Eq. (5) results in

$$\alpha_U \approx \beta_u \alpha_u + \beta_v \alpha_v. \quad (9)$$

The terms α_u and α_v are the coefficients obtained by linear regression of Niño-3 zonal wind speed and meridional wind speed seasonal anomalies on SSTAs, respectively; $\beta_u \alpha_u$ can be taken as the contribution of
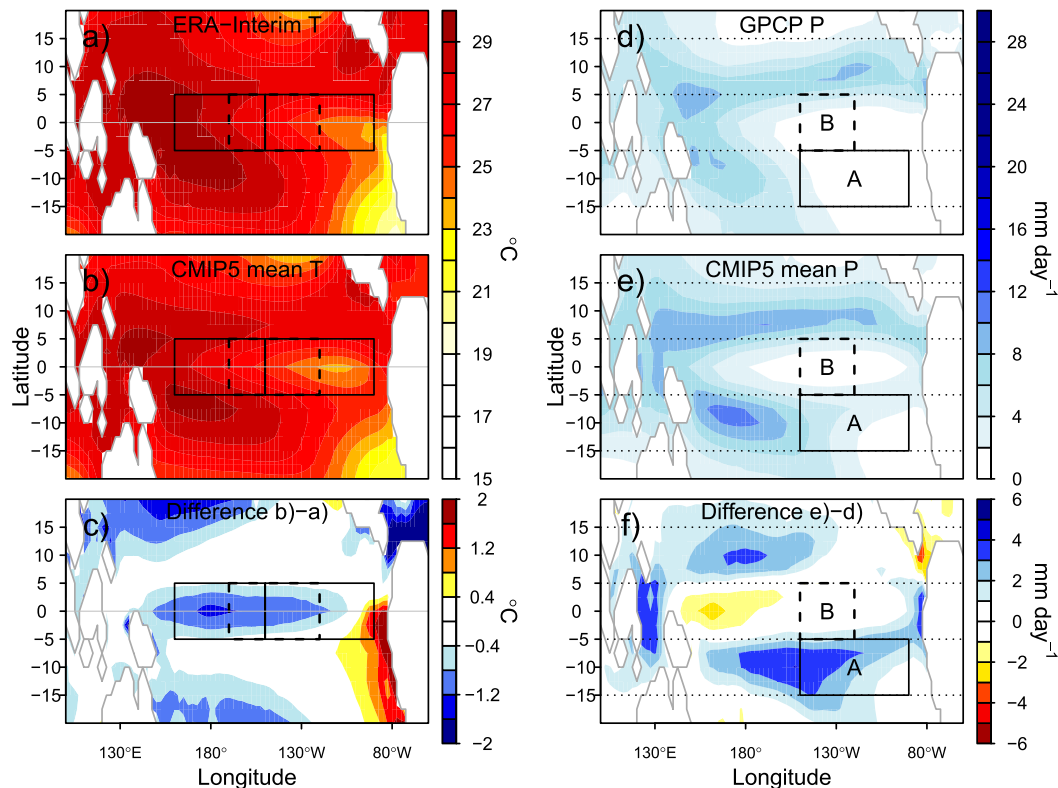
FIG. 1. (a) Time-mean SST for ERA-Interim; (b) as in (a), but for the CMIP5 ensemble mean; (c) the difference between (a) and (b); (d) time-mean precipitation for GPCP; (e) as in (d), but for the CMIP5 ensemble mean; (f) the difference between (d) and (e). In (a)–(c) the Niño-3 (east) and Niño-4 (west) regions are outlined by solid boxes and Niño-3.4 outlined by a dashed box. In (d)–(f) the southeast Pacific region is outlined in solid lines and the southeast equatorial region outlined by a dashed line. Dotted lines also show the north, equator, and south bands corresponding to Fig. 3.

zonal wind speed anomalies to wind speed feedback (α_U) and $\beta_v \alpha_v$ is the meridional wind speed contribution. Once again, seasonal anomalies of u, v, and U are constructed from mean daily fields. For ease, these components will be referred to as the zonal and meridional wind speed feedbacks throughout.

A measure to quantify the symmetry of the ENSO precipitation response about the equator is also used. This is found by taking the difference between the South Pacific precipitation feedback (precipitation seasonal anomalies averaged over 5°–15°S, 170°–120°W regressed on Niño-3 SSTAs) and North Pacific precipitation feedback (latitude 5°–15°N, same longitude).

4. Equatorial Pacific precipitation and SST in CMIP5

Observed annual and time mean temperatures in the equatorial Pacific are cooler in the east and warmer in the west (Fig. 1a). This zonal surface temperature gradient reinforces atmospheric circulation along the equator in the Pacific (i.e., the Walker circulation).

Trade winds blow along the equator from the high pressure cooler region in the east (cold tongue) to the low pressure warmer west Pacific region (warm pool). Here, air rises and is advected toward the east Pacific at higher altitudes to sink over the cold tongue, completing the Walker circulation.

Coupled climate models tend to suffer from the cold tongue bias (Lin 2007; Bellenger et al. 2014; Zhang et al. 2015), a bias characterized by sea surface temperatures (SSTs) being too cool along the equator (e.g., Figs 1b,c). A second common bias lies with precipitation, in the form of the double-ITCZ bias. The equatorial Pacific features most precipitation and atmospheric ascent (measured in Fig. 3 by pressure tendency at the 500-hPa pressure level; e.g., Bony et al. 1997) over the warm pool where the ascending branch of the Walker circulation is located. There is also a band of precipitation to the north of the equator, the ITCZ (Fig. 1d), indicating the low-level convergence of air (the Hadley cell). Similarly, a smaller area of atmospheric ascent and precipitation exists to the southwest in the South Pacific convergence

zone (SPCZ). This region of precipitation in CMIP5 models tends to be too zonally oriented and to extend too far to the east compared to the observations (Figs. 1e,f), hence the name "double ITCZ." There is also insufficient precipitation along much of the equatorial Pacific as the ascending branch of the Walker circulation tends to be located farther west.

The ensemble mean analysis in Fig. 1 identifies three zonal bands, isolating the regions that are most important to these temperature and precipitation biases, the northern, equatorial, and southern bands (dotted lines on these figures). All three bands show discrepancies between the observed and CMIP5 ensemble mean precipitation, while the equatorial band shows the largest SST biases. These bands can consequently be used to more quantitatively identify the extent and diversity of the SST and precipitation biases in this subset of CMIP5 models.

The equatorial average (latitude 5°S–5°N) of SSTs shows the presence of the cold tongue bias to varying extents in many of the CMIP5 models in this study (Fig. 2a). CSIRO Mk3.6.0 (CMIP5 model 4, hereinafter simply CMIP5 4, and so on for others; see model numbers in Table 1) in particular, shown in red in figures, shows cool mean SSTs along the equator compared to ERA-Interim. However, some models show temperatures closer to ERA-Interim. In fact, CanESM2 (CMIP5 3, yellow), IPSL-CM5B-LR (CMIP5 7c, brown) and MIROC4h (CMIP5 8a, light green) have warmer Niño-3 (N3) temperatures (mean N3 temperatures of 26.0°, 26.5°, and 26.8°C, respectively) than observed (ERA-Interim has a mean N3 temperature of 25.9°C).

The standard deviation of SSTAs indicates the strength and zonal location of El Niño/La Niña events along the equator. In ERA-Interim, anomalies are strongest in the east equatorial Pacific (Fig. 2b). SSTA variability strength and spatial pattern are known to vary significantly among coupled climate models (AchutaRao and Sperber 2006; Capotondi et al. 2006; Guilyardi 2006; Bellenger et al. 2014). The east Pacific peak shown by the reanalysis is replicated by many of the CMIP5 models used here but at varying strengths. Some models feature a stronger peak in the Niño-3 region than in observations, e.g., BCC_CSM1.1(m), BNU-ESM, GFDL-ESM2M, and MIROC5. However, two models, MIROC4h and CSIRO Mk3.6.0, show SSTA standard deviation (SD) maxima located farther to the west. Generally, models used in this study display a range of temperature variability in the east Pacific with no consistent bias among the models as demonstrated by the standard deviation of Niño-3 SSTAs (Table 2).

As well as the extent of the cold tongue bias, the spatial distribution of mean precipitation and atmospheric ascent
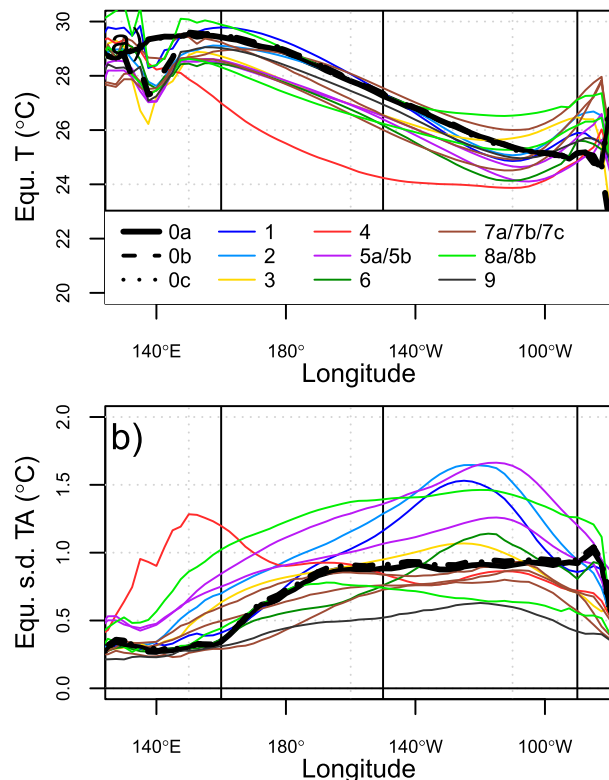

FIG. 2. Equatorial mean (averaged over 5°S–5°N) (a) time-mean SST and (b) standard deviation of SSTAs as a function of longitude for observation datasets and CMIP5 models (See Table 1 for the model and dataset numbering). Niño-4 (160°E–150°W) and Niño-3 (150°–90°W) longitude bands are shown using vertical black lines.

are also examined to assess the presence of the double-ITCZ bias in the CMIP5 models. All three bands are examined (Fig. 3) as various characteristics of atmospheric circulation and the double-ITCZ bias are displayed in all three regions (Figs. 1d,f). For the CMIP5 models, precipitation along the equatorial Pacific tends to be insufficient, with the maximum precipitation shifted westward due to a westward shift of the Walker circulation compared with the reanalysis (Figs. 1f and 3c). This is most evident in CSIRO Mk3.6.0, the model found to show the largest SST bias, and is consistent with the cold tongue bias identified in Fig. 2. An outlier is MIROC5, which shows more precipitation along the equator than the reanalysis, although it still has a maximum farther to the west. MIROC5 also shows a stronger cool temperature bias to the south of the equator than along the equator, unlike some of the other CMIP5 models, which may explain this discrepancy. CMIP5 models tend to show a stronger ITCZ (more precipitation and ascent; Figs. 3a,b) to the west and a weaker ITCZ toward the east, past ~130°W. Models often show more precipitation and atmospheric ascent in the south (Figs. 3e,f) with precipitation and atmospheric ascent extending

TABLE 2. Latent heat flux damping (α_{LH}), humidity gradient feedback ($\alpha_{\Delta q}$), wind speed feedback (α_U), and standard deviation of Niño-3 SSTA for reanalyses and CMIP5 models detailed in Table 1. Differences from the OAFlux dataset are given in parentheses. Differences in bold indicate when a model feedback's 95% confidence interval is outside of the confidence interval for the reanalysis.

No.	α_{LH}	$\alpha_{\Delta q}$	α_U	SD SSTA (N3)
0a	-9.72 ± 1.04	-9.62 ± 0.82	-1.13 ± 0.94	0.84
0b	-11.81 ± 1.90	-7.99 ± 0.97	$+1.92 \pm 1.55$	0.88
0c	-10.89 ± 1.33	-11.15 ± 0.83	$+0.51 \pm 1.21$	0.86
1	**-8.09 ± 0.40 (+1.63)**	**-8.49 ± 0.23 (+1.14)**	-0.52 ± 0.42 (+0.61)	1.22 (+0.37)
2	**-8.24 ± 0.43 (+1.47)**	**-11.61 ± 0.53 (−1.98)**	**1.27 ± 0.59 (+2.40)**	1.37 (+0.52)
3	**-6.94 ± 0.55 (+2.77)**	-10.09 ± 0.44 (−0.46)	**3.05 ± 0.56 (+4.17)**	0.92 (+0.07)
4	**-5.89 ± 0.63 (+3.83)**	**-7.72 ± 0.41 (+1.90)**	**1.75 ± 0.67 (+2.88)**	0.73 (−0.12)
5a	**-8.56 ± 0.52 (+1.16)**	**-11.92 ± 0.56 (−2.29)**	**1.43 ± 0.47 (+2.55)**	1.08 (+0.24)
5b	**-8.53 ± 0.58 (+1.19)**	**-11.51 ± 0.54 (−1.89)**	**1.81 ± 0.52 (+2.93)**	1.42 (+0.58)
6	**-7.32 ± 0.56 (+2.40)**	-9.39 ± 0.61 (+0.24)	**1.87 ± 0.73 (+3.00)**	0.85 (+0.01)
7a	**-4.70 ± 0.55 (+5.01)**	**-7.23 ± 0.44 (+2.40)**	**2.83 ± 0.63 (+3.96)**	0.73 (−0.11)
7b	**-6.57 ± 0.50 (+3.14)**	**-8.08 ± 0.46 (+1.55)**	**1.53 ± 0.59 (+2.66)**	0.78 (−0.07)
7c	**-6.57 ± 0.70 (+3.14)**	-9.64 ± 0.60 (−0.01)	**3.36 ± 0.74 (+4.49)**	0.69 (−0.15)
8a	**-6.15 ± 0.72 (+3.56)**	-10.81 ± 0.59 (−1.19)	**4.22 ± 0.67 (+5.34)**	0.59 (−0.25)
8b	**-4.20 ± 0.73 (+5.52)**	-11.04 ± 0.47 (−1.42)	**6.00 ± 0.84 (+7.13)**	1.34 (+0.50)
9	**-6.76 ± 0.89 (+2.96)**	-9.76 ± 0.80 (−0.13)	**3.01 ± 0.79 (+4.14)**	0.50 (−0.35)

farther to the southeast (SE) than observed. This extended band of precipitation will be referred to throughout as the SE ITCZ. There is a relatively large spread in the representation of the zonal extent of the SE ITCZ in the CMIP5 models. CSIRO Mk3.6.0 again shows larger biases, with a more extended SE ITCZ and strong northwest precipitation and ascent compared with other models and the reanalysis. Once again, the MIROC5 model shows less precipitation and atmospheric ascent than other CMIP5 models in the South Pacific band.

It is established here that the CMIP5 models in this study have a diverse representation of ENSO behavior and significant biases in the mean equatorial Pacific climate. The biases and diversity in the mean atmospheric circulation shown here are likely to have links to other aspects of the equatorial Pacific, such as the trade winds, as well as atmospheric feedbacks governing the diversity of ENSO-related variability.

Equatorial Pacific precipitation and overlaid wind fields for the ERA-Interim reanalysis data and two CMIP5 models are displayed in Fig. 4. The two models were selected to represent the range of the double-ITCZ bias in the ensemble. Both the time mean fields and El Niño composites are given to examine the possible impact of varying atmospheric circulation on mean surface winds and on El Niño variability. The observed mean atmospheric circulation shows southeasterly winds along the equator, converging onto the ITCZ (Fig. 4a). The observed El Niño composite (Fig. 4b) shows a southward shift of the ITCZ, a slight northeastward shift of the southwest Pacific precipitation, and an eastward shift of the ascending branch of the Walker circulation.

The meridional circulation shifts coincide with northerly wind speed anomalies (shown by red arrows on Fig. 4b) north of the equator and southerly anomalies south of the equator. The zonal shifts are linked to westerly wind anomalies in the west Pacific. These wind responses play an important role in ENSO feedbacks by amplifying (via impacts on oceanic dynamic processes) and damping (via impacts on evaporative heat flux) east Pacific SSTAs.

The variation of mean atmospheric circulation between models can relate to the mean meridional winds along the equator (Figs. 4c,e). In contrast to the observed winds, the extended SE ITCZ in some models results in a contrast in the meridional wind direction either side of the equator. These models show southeasterly winds to the north of the equator and regions of northeasterly winds to the south of the equator (e.g., Fig. 4c) as winds also converge onto the SE ITCZ. The central Pacific region labeled B will be used in later discussion to quantify meridional wind variation among models. The difference in background mean state between models may be linked to diversity in the ENSO wind speed feedback, a contributor to El Niño–related variability via its impact on latent heat flux.

In contrast to the observed response, the El Niño composite wind speed in CMIP5 models is largely dominated by a strengthening SE ITCZ because of the increased zonal extent of the mean SE ITCZ. This primarily causes northwesterly wind anomalies (shown by red arrows in Figs. 4d,f) as winds converge onto the farther extended SE ITCZ in the southeast. This either enhances or reduces the wind speed based on the background wind speed direction as mentioned above,
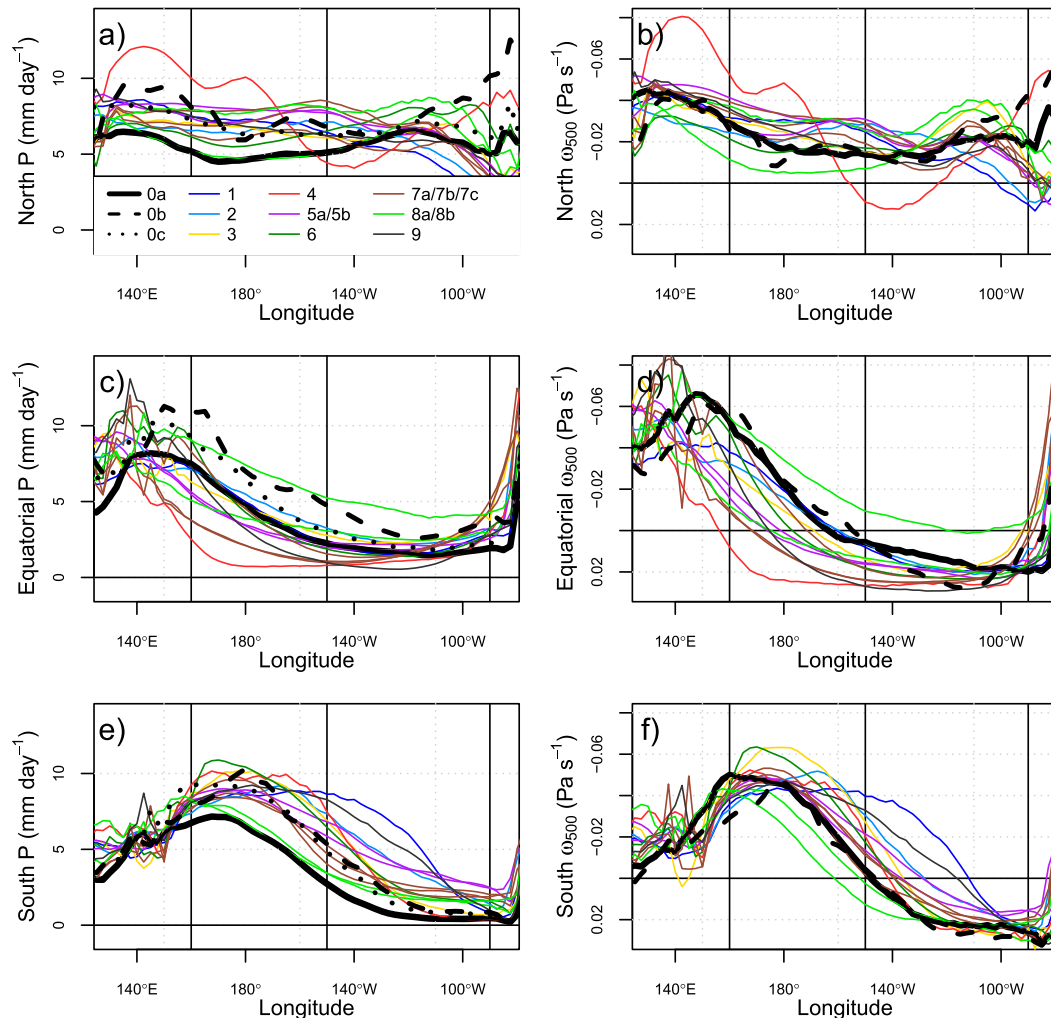
FIG. 3. (a) Observed and CMIP5 mean precipitation as a function of longitude averaged over the North Pacific (5°–15°N). (b) As in (a), but for vertical velocity (pressure tendency, ω) at 500 hPa. (c),(d) As in (a),(b), but averaged over the equator (5°S–5°N). (e),(f) As in (a),(b), but averaged over the South Pacific (5°S–15°S). Niño-4 (160°E–150°W) and Niño-3 (150°–90°W) are shown using vertical black lines.

likely resulting in diversity in the CMIP5 wind speed feedbacks and hence LHF damping. Xie and Philander (1994) identified the impact of surface winds on the LHF–SST feedback. They introduced the wind–evaporation–SST (WES) feedback and proposed this to be a possible cause of the meridional precipitation asymmetry about the equator. They describe a meridional dipole of SST perturbations (positive SSTA to the north of the equator and negative SSTA to the south of the equator), resulting in anomalous southerly winds. As a result of the Coriolis force, anomalous winds are easterly in the south and westerly in the north, increasing and decreasing the initial easterly winds respectively (an example of this can be seen in Figs. 4d and 4f). This causes increased evaporation in the south and decreased evaporation in the north, reinforcing the

initial SST anomaly. In this case, the initial meridional winds are also of importance to the impact of anomalous winds on SST. For example, during an El Niño in a model with a more extended SE ITCZ (Figs. 4e,f), the northerly meridional winds south of the equator are amplified. Conversely, models with a weaker SE ITCZ have more southerly meridional winds (Fig. 4d) that will then be weakened, reducing evaporation. Similarly, the contrast in anomalous wind direction shown in the CMIP5 El Niño composites compared to the observed El Niño composite is likely to result in a difference between the CMIP5 and reanalysis wind speed feedbacks.

Examining these differences, it seems likely that diversity in the model mean state may be linked to variation in atmospheric feedbacks, such as the latent heat flux damping, via its relationship to convective
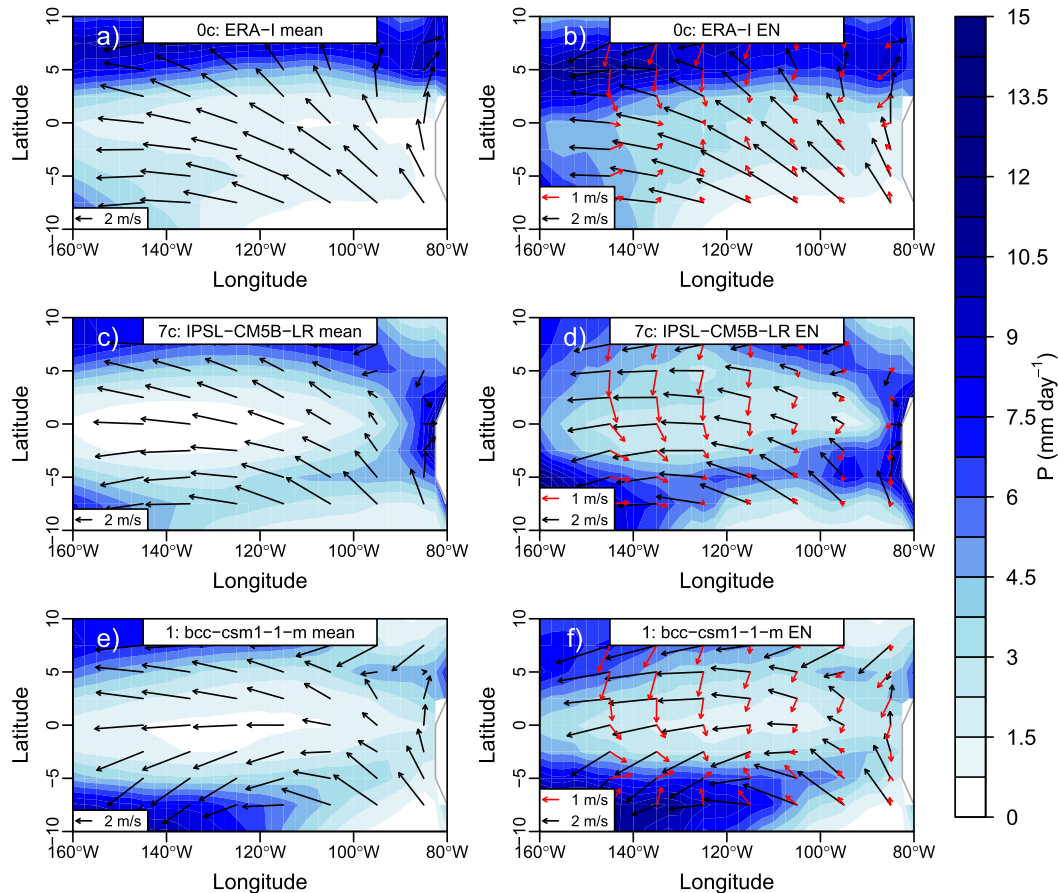
FIG. 4. (a) Time-mean equatorial Pacific precipitation for ERA-Interim. (b) El Niño composite precipitation for ERA-Interim. (c),(d) As in (a),(b), but for IPSL-CM5B-LR (CMIP5 7c), a model with less double-ITCZ bias. (e),(f) As in (a),(b), but for BCC_CSM1.1(m) (CMIP5 1), a model with a larger double-ITCZ bias. Mean surface wind vectors are plotted using black arrows on the figures. El Niño composites of surface wind speed anomalies are plotted using red arrows in (b), (d), and (f).

responses and wind speed feedbacks. The remainder of this study identifies and implements metrics that can be used to quantify these mean state and feedback biases and their relation to one another in the CMIP5 models.

5. The relationship between mean atmospheric circulation and ENSO atmospheric feedbacks

a. ENSO atmospheric feedback diversity in CMIP5

Latent heat flux damping is one of the dominant components of ENSO thermodynamic damping, weakening El Niño and La Niña events via anomalous heat flux, and is quantified as the linear regression coefficient of latent heat flux anomalies against SSTAs in Niño-3 [Eq. (3)]. Latent heat is the heat flux due to evaporation and can be decomposed into a wind speed component and a near-surface humidity gradient component [Eq. (6)]. Latent heat flux anomalies in the east equatorial

Pacific, the area most important to ENSO as this is where SSTAs are typically largest (Fig. 2b), tend to be dominated by near-surface humidity difference. This is demonstrated by the relative strengths of the two latent heat damping components in Fig. 5. The three reanalyses, OAFlux, NCEP, and ERA-Interim, have LHF dampings (α_{LH}) with dominant humidity feedbacks ($\alpha_{\Delta q}$) accounting for most of the total LHF damping (Table 1).

Wind speed (WS) feedbacks (α_U) are smaller and show differences in sign depending on the reanalysis. OAFlux is the only reanalysis with a WS feedback significantly different from zero [a significant difference here is defined when the 95% confidence interval of the regression coefficient falls outside the confidence interval of the linear fit for the feedback; e.g., Eq. (3)]. NCEP and ERA-Interim have positive WS feedbacks not significantly different from zero. Figure 5 also shows the LHF damping calculated using the latent heat flux
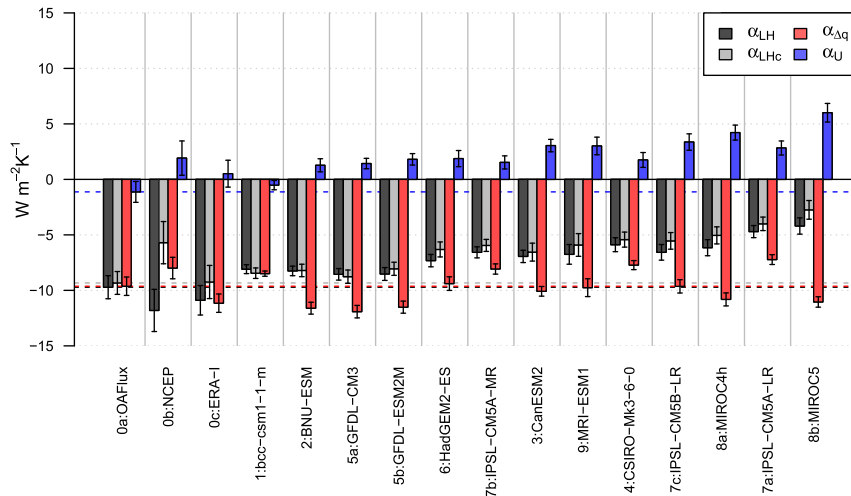
FIG. 5. Reanalysis and CMIP5 Niño-3 latent heat damping calculated using the latent heat flux field given by the model/dataset (α_{LH}, dark gray bars), latent heat damping calculated using latent heat flux reconstructed using bulk formula (α_{LHc}, light gray bars), humidity anomaly component of α_{LH} ($\alpha_{\Delta q}$, red bars), and the wind speed anomaly component of α_{LH} (α_U, blue bars). Error bars show the 95% confidence interval from the linear fit of the feedbacks. CMIP5 models are ordered by the magnitude of RMSE of the four values against OAFlux values, from lowest RMSE on the left to highest.

field constructed using the bulk formula [Eq. (1)] and the model wind speed and humidity gradient fields, labeled α_{LHc} to allow comparison of the model output LHF damping (calculated from monthly output) and the decomposition LHF damping (calculated from daily output). It is important to note that the NCEP reanalysis shows a significant difference between the LHF damping calculated using the reanalysis latent heat flux field and the LHF damping calculated using the bulk formula (α_{LHc}). This may be a result of an identified issue of the bulk formula algorithm used in the NCEP-2 dataset. NCEP datasets have latent heat flux that tends to be higher in high heat flux conditions (Moore and Renfrew 2002; Renfrew et al. 2002; Kubota et al. 2008) as a result of the roughness length formulation (see Figs. 5 and 6 of Moore and Renfrew 2002). Using an alternative bulk formula algorithm has been shown to give significantly different latent heat flux (Brunke et al. 2002; Kubota et al. 2008). This discrepancy means that the latent heat flux decomposition is unsuitable to be used for this reanalysis, although we include NCEP-2 in figures for reference. Because of the closeness of α_{LH} and α_{LHc} for OAFlux, this is the dataset that will be used as the reanalysis reference in discussions comparing the CMIP5 ensemble and observations. ERA-Interim is used when examining individual zonal and meridional WS feedbacks as OAFlux zonal and meridional wind speeds are unavailable.

All models show a LHF damping weaker than OAFlux, although three models, BNU-ESM (CMIP5 2) and both GFDL models (CMIP5 5a and 5b), do not

show a difference outside of the 95% confidence intervals given by the linear fits of α_{LH}. Bellenger et al. (2014) find that this bias persists for many members of the CMIP5 ensemble. A relatively consistent bias of this subensemble is a too strong positive Niño-3 WS feedback with all but one model [BCC_CSM1.1(m)] showing a WS feedback significantly biased compared to OAFlux (Table 2). In contrast to this, the dominant humidity gradient feedback shows differing biases between models. Eight models show a strong humidity feedback, with four of these being significantly different from the reanalysis (BNU-ESM, GFDL CM3, GFDL-ESM2M, and MIROC5). The remaining seven models show a weak humidity feedback, with BCC_CSM1.1(m), CSIRO Mk3.6.0, IPSL-CM5A-LR, and IPSL-CM5A-MR showing a significant positive bias. This diversity means that the overall causes of LHF damping bias differ for each model, as was suggested by Lloyd et al. (2011) to be the case for CMIP3 models. The bias in LHF damping for BCC-BSM1.1(m) lies largely with a weak humidity feedback. Biases in CanESM2, HadGEM2-ES, IPSL-CM5B-LR, MIROC4h, and MRI-ESM1 are the result of a too strong positive WS feedback. CSIRO Mk3.6.0, IPSL-CM5A-LR, and IPSL-CM5A-MR have weak latent heat flux feedbacks due to both weak humidity feedbacks and strong WS feedbacks. The remaining models, BNU-ESM, GFDL CM3, and GFDL-ESM2M, show no significant bias in total LHF damping but all show strong humidity feedbacks and strong negative WS feedbacks, resulting in little bias
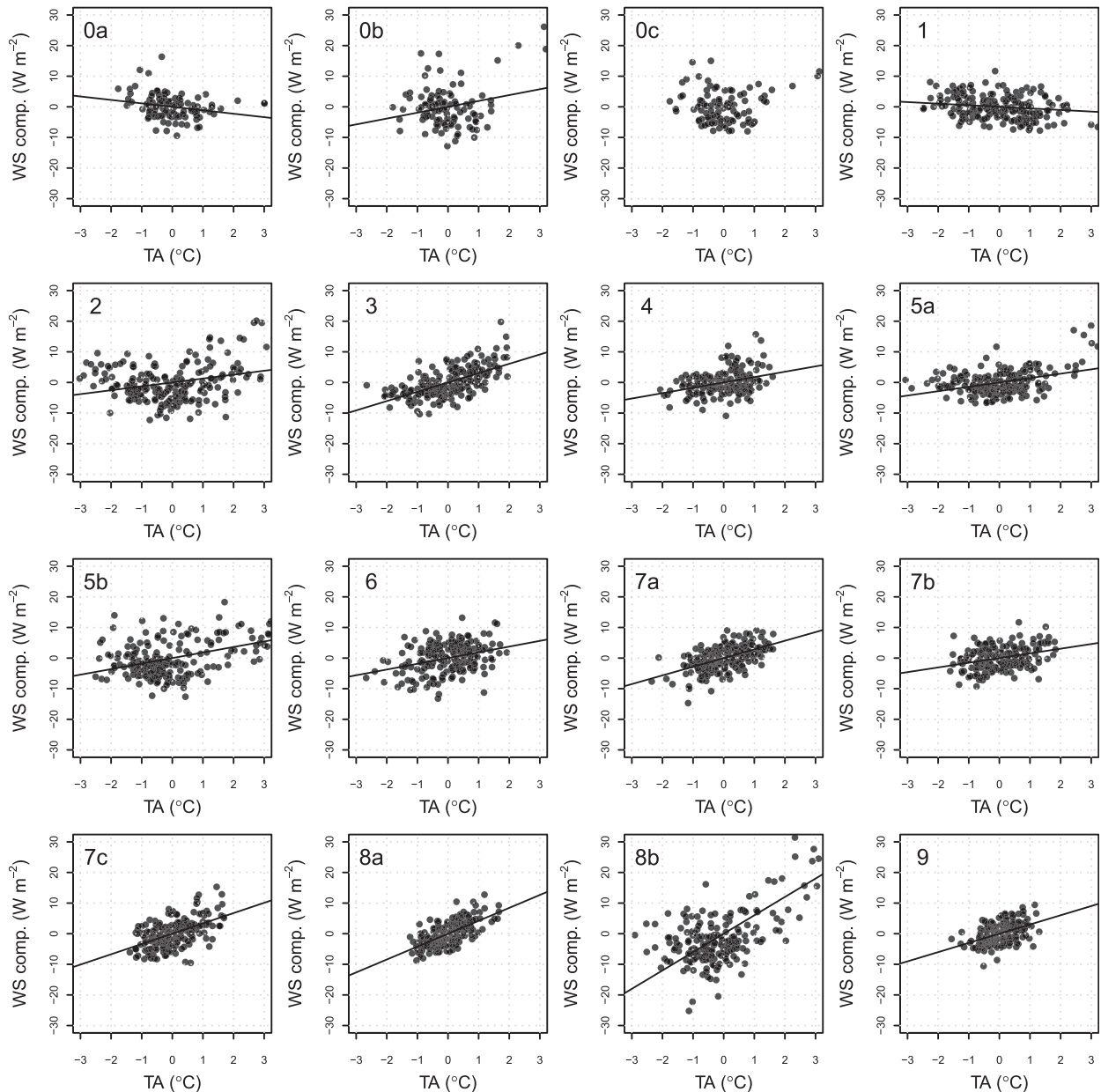
FIG. 6. Wind speed anomaly component of Niño-3 latent heat flux seasonal anomalies (*y* axis) plotted against Niño-3 seasonal SSTAs (*x* axis) for reanalyses (0a–0c) and CMIP5 models (1–9). See Table 1 for the model and dataset numbering. Black lines on the figures show the linear fits for the wind speed feedback (α_U) values that are at least 95% significant. A solid line is used for a linear fit that is 95% significant.

overall. A measure of the accuracy of the modeled α_{LH} is found by taking the RMSE of all four LHF damping measures (α_{LH}, α_{LHc}, $\alpha_{\Delta q}$ and α_U) for each CMIP5 model with the reanalysis. Kim et al. (2014a) previously used RMSE in this way to assess the accuracy of the relative strength of ENSO feedbacks in an ENSO stability analysis. BCC_CSM1.1(m) shows the lowest RMSE of $1.1\,\mathrm{W\,m^{-2}\,K^{-1}}$ and MIROC5 shows the largest RMSE ($5.6\,\mathrm{W\,m^{-2}\,K^{-1}}$) due to a large humidity feedback and a comparatively strong positive WS

feedback. The CMIP5 models in Fig. 5 are ordered by latent heat damping accuracy using this measure.

Significant biases in the WS feedback are found in almost all CMIP5 models. The linear fits for the WS feedback (Fig. 6) show the discrepancy between the observed wind speed response to SSTAs and many of the modeled wind speed responses. The OAFlux reanalysis shows a 95% significant positive relationship between the wind speed component of latent heat flux and Niño-3 SST anomalies (0a in Fig. 6). However, the
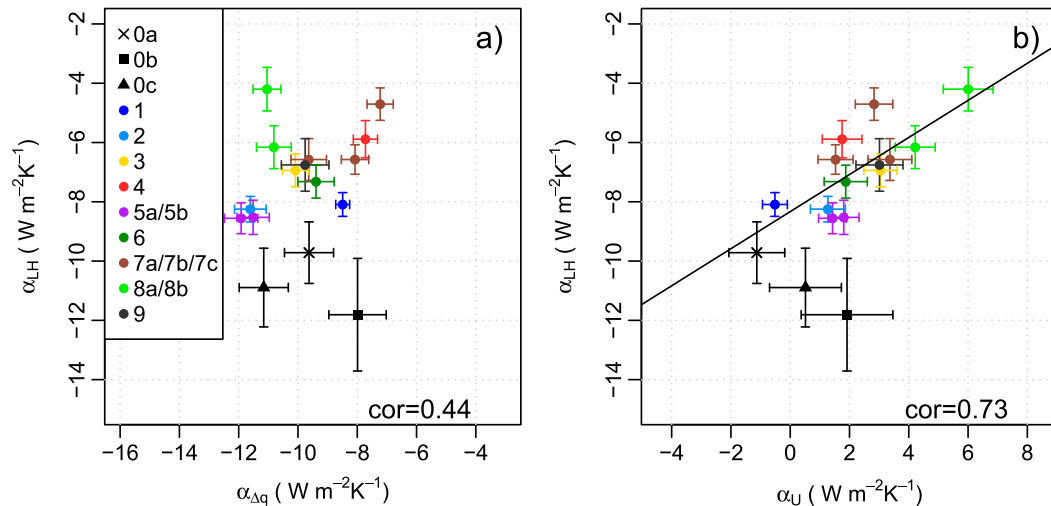
FIG. 7. (a) Reanalysis and CMIP5 latent heat damping (α_{LH}; y axis) against the humidity anomaly component ($\alpha_{\Delta q}$; x axis). (b) As in (a), but with the wind speed anomaly component (α_U) on the x axis. Error bars show the 95% confidence interval from the linear fit of the feedbacks. Relationships significant at the 95% level by the Student's t test are shown by a solid black linear fit line and correlations for the 13 CMIP5 models are shown at the bottom right.

slope of the fit (WS feedback) is relatively small and not significantly different from zero (Table 1). Figure 6 shows that at higher temperatures (i.e., during more extreme El Niño events) wind speeds begin to decrease or show less response than at lower temperatures, demonstrating a nonlinear response of surface winds to SSTAs. This is in agreement with Zhang and McPhaden (1995), who demonstrated this behavior of equatorial Pacific wind speed in response to SST. This response is more pronounced in the ERA-Interim reanalysis (0c in Fig. 6) with decreasing winds at both positive and negative SSTAs, contributing to increasing evaporation. This results in an insignificant (positive; 95% level) fit for the ERA-Interim WS feedback. This feedback response is indicative of the well-documented asymmetric nature of ENSO (e.g., Dommenget et al. 2013).

In contrast to the reanalyses, almost all models show more linear wind speed responses to SSTAs and have significant positive WS feedbacks. BCC.CSM1.1(m) is an exception in which wind speed anomalies are relatively weak, resulting in a small negative feedback. Some models show a slightly stronger weakening of winds in response to larger positive SSTAs, such as BNU-ESM (CMIP5 2) and GFDL CM3 (CMIP5 5a). Notably, BNU-ESM also shows reduced wind speeds at negative SSTAs. However, the increased wind speeds at lower temperatures shown in the majority of CMIP5 models seem to be the primary difference between the CMIP5 and reanalysis wind speed feedbacks, meaning that the models tend to have a stronger positive feedback.

Figure 6 suggests that the inability of coupled climate models to replicate the observed El Niño–La Niña asymmetry (Philip and van Oldenborgh 2009; Choi et al. 2013; Dommenget et al. 2013; Zhang and Sun 2014) may be an underlying cause of LHF damping bias. Despite this, it is found that there is no significant difference between LHF damping calculated for only positive SST anomalies (feedback during El Niño) and LHF damping calculated for only negative SST anomalies (feedback during La Niña) in the three observed datasets. Therefore, it seems that nonlinearity of the wind speed response, as shown in Fig. 6, does not have a large impact on the linearity of LHF damping. Furthermore, the strength of the nonlinearity of the wind speed response is also not significantly related to variation in the strength of the LHF damping.

While it is established that variations in humidity are most important for controlling interannual latent heat flux variability in the east Pacific in individual models, the importance of the wind speed feedback in the LHF damping bias for many of the CMIP5 models suggests that the humidity feedback may not be the most important feedback when considering interensemble α_{LH} variations. This is confirmed by examining the correlations between LHF damping and the wind speed (α_U) and humidity gradient ($\alpha_{\Delta q}$) feedbacks (Fig. 7). The correlation between α_{LH} and $\alpha_{\Delta q}$ is insignificant with a correlation of -0.44 (Fig. 7a). It is important to note that an outlying model (MIROC5) seems to be a possible cause of this. Indeed, when this model is removed the correlation is increased to -0.72 (significant at the 95%
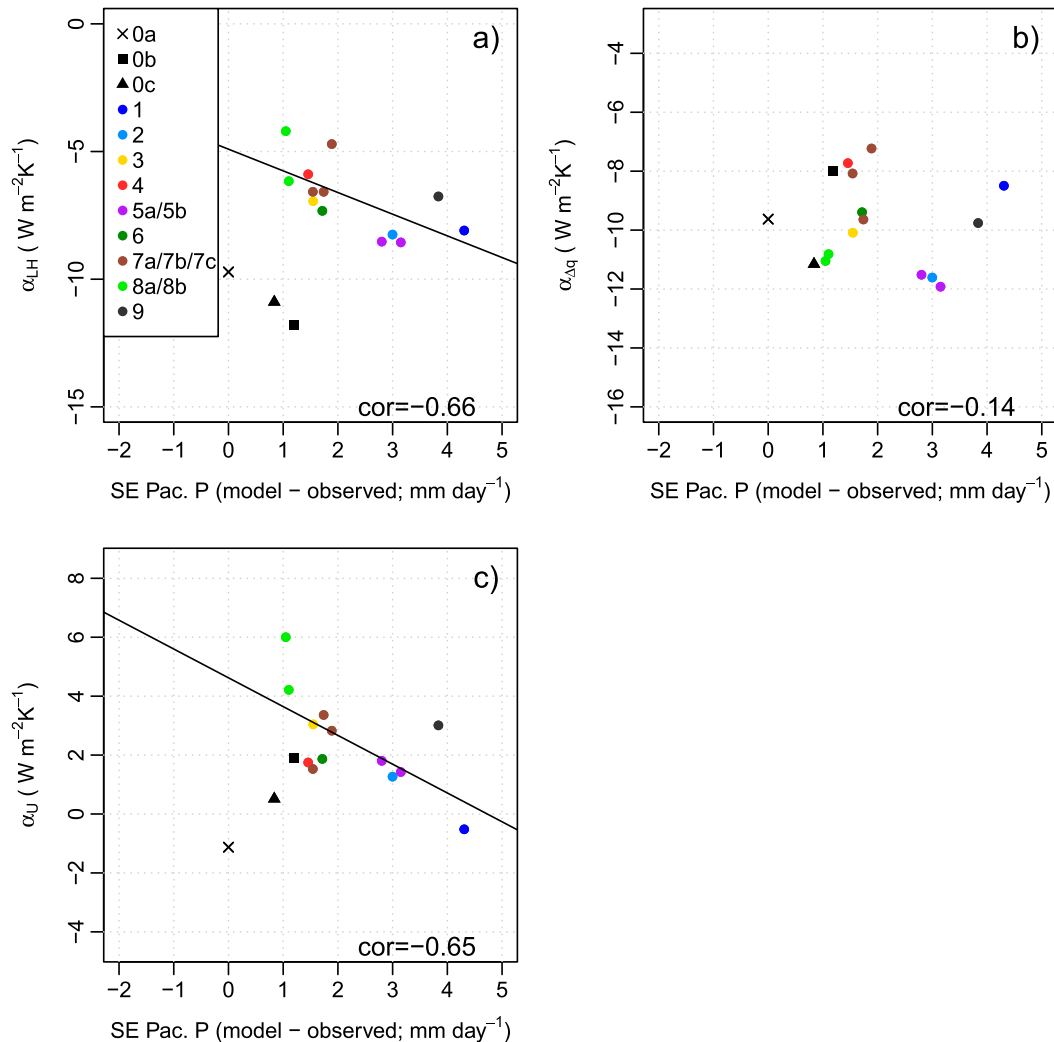
FIG. 8. (a) Reanalysis and CMIP5 Niño-3 latent heat damping (α_{LH}; y axis) against the southeast Pacific (region A; longitude 150°–90°W, latitude 5°–15°S) precipitation bias (x axis). (b) As in (a), but with the humidity anomaly component ($\alpha_{\Delta q}$) on the y axis. (c) As in (a), but with the wind speed anomaly component (α_U) on the y axis. Relationships significant at the 95% level by the Student's t test are shown by a black linear fit line and correlations for the 13 CMIP5 models are shown at the bottom right.

level). The correlation between α_{LH} and α_U (Fig. 7b) is −0.73, suggesting that interensemble variation of wind speed feedback strength is also an important factor in the diversity of latent heat flux damping strength. The underlying causes of the interensemble diversity of these feedbacks are examined further in the following section.

b. Double-ITCZ diversity in relation to ENSO atmospheric feedbacks

We previously hypothesized that diversity in the mean atmospheric circulation may be linked to LHF damping via its other atmospheric feedbacks. Taking southeast Pacific (region A in Fig. 4; 15°–5°S, 150°–90°W) precipitation bias (difference between model and observed precipitation) as a measure of the double-ITCZ bias/SE

ITCZ diversity (e.g., Figs. 1f and 3e) and correlating this with LHF damping supports this hypothesis; a correlation of −0.66 is found between the two (Fig. 8a). Models with a more extended SE ITCZ have a stronger LHF damping and, conversely, a weaker SE ITCZ coincides with a weaker LHF damping. The underlying cause of this relationship can be found by also examining the relation between the SE ITCZ and the wind speed and humidity gradient feedbacks. The zonal extent of the SE ITCZ and the wind speed feedback are negatively related with a correlation of −0.65 (Fig. 8c), showing that models with a more pronounced SE ITCZ have a weaker positive or even negative wind speed feedback on SSTA, resulting in a stronger LHF damping. Note here that observations do not fit the interensemble
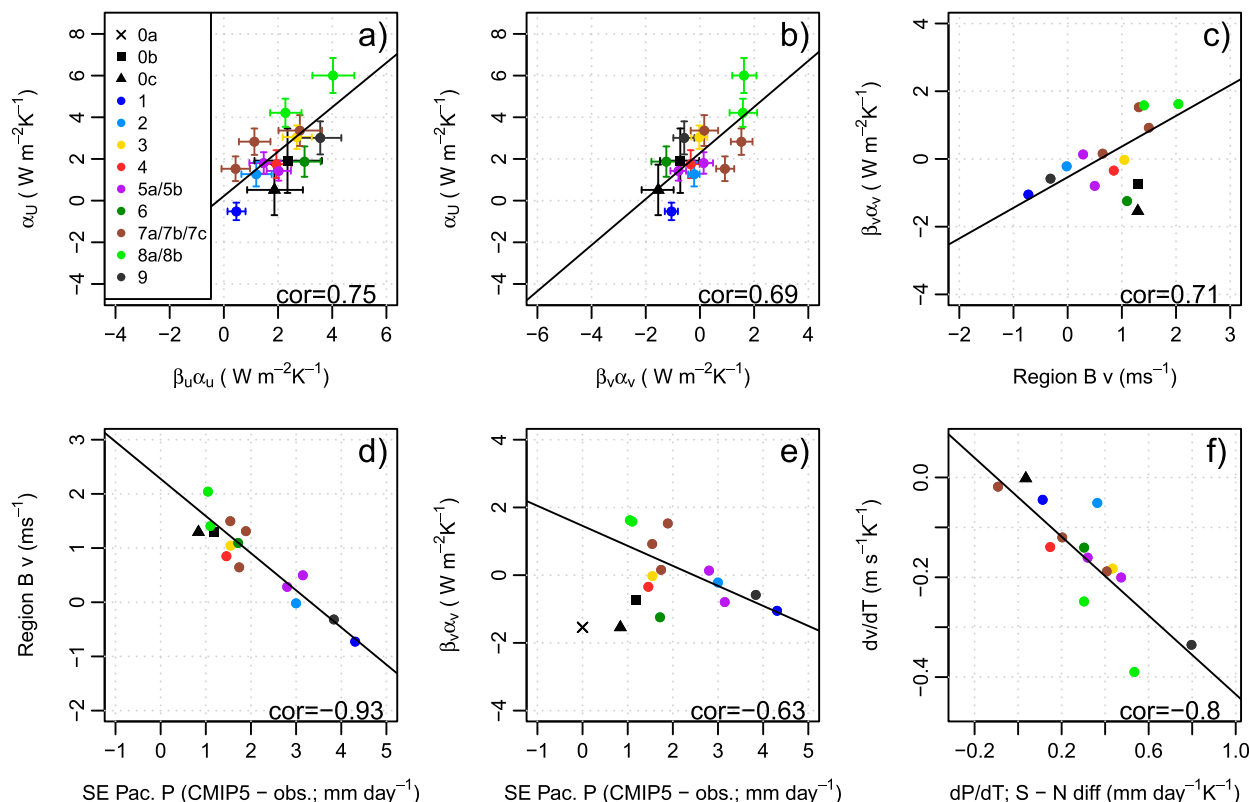
FIG. 9. (a) Reanalysis and CMIP5 total wind speed feedback (α_U) against zonal wind speed feedback ($\beta_u\alpha_u$). (b) As in (a), but with meridional wind speed feedback ($\beta_v\alpha_v$) on the *x* axis. (c) Meridional wind speed feedback against meridional wind averaged over region B (longitude 150°–120°W, latitude 5°S–5°N). (d) Mean region B meridional wind speed against southeast Pacific precipitation bias. (e) As in (c), but with mean southeast Pacific (longitude 150°–90°W, latitude 5°–15°S) precipitation bias on the *x* axis. (f) Niño-3 meridional wind feedback (*dv/dT*, Niño-3 meridional wind anomalies regressed on SSTAs) plotted against the difference between south (longitude 170°–120°W, latitude 5°–15°S) and north (same longitude, latitude 5°–15°N) precipitation feedbacks (precipitation anomalies regressed on Niño-3 SSTAs). Relationships significant at the 95% level by the Student's *t* test are shown by a black linear fit line. Correlations for the 13 CMIP5 models are shown at the bottom right. Point 0a in (c) uses ERA-Interim (0c) feedback values because meridional winds are not provided for OAFlux.

relationship well, suggesting that other processes, aside from the mean state, may also be important to feedback bias. This is revisited in later figures.

The relationship between the humidity gradient feedback and southeast Pacific precipitation is insignificant (correlation −0.14; Fig. 8b). This is because humidity gradient anomalies are more driven by atmospheric circulation responses along the equator; a correlation of −0.56 is found between the humidity feedback and Niño-4 precipitation (not shown in figures). A relationship is also found between humidity feedback and mean SST in the central equatorial Pacific. Surface specific humidity (q_s) is a function of SST (see section 3). At higher SSTs, the response of surface specific humidity to SSTA increases, resulting in the negative relationship between $\alpha_{\Delta q}$ and the mean conditions along the equator.

These results imply that the interensemble diversity in LHF damping strength is at least partially related to atmospheric circulation biases via variations in the wind

speed feedback, as opposed to humidity gradient feedback diversity. The contribution of zonal and meridional wind speed anomalies to the total WS feedback is examined to further identify the dynamics governing the relationship between latent heat flux damping and mean atmospheric circulation.

The diversity in WS feedback strength (α_U) is, as might be expected, strongly influenced by both zonal ($\beta_u\alpha_u$) and meridional ($\beta_v\alpha_v$) WS feedbacks, with correlations of 0.75 and 0.69, respectively (Figs. 9a,b). The zonal WS feedback (Fig. 9a) tends to be the strongest positive component, showing weakening zonal winds in response to positive SSTAs (the Bjerknes feedback). Few models show significant bias in the zonal WS feedback (Fig. 9a; Table 3). Five show a weak positive feedback [only BCC_CSM1.1(m) is significantly different from ERA-Interim]. The remaining models have a stronger positive feedback (only MIROC5 is significantly stronger than ERA-Interim).

TABLE 3. Zonal $(\beta_u\alpha_u)$ and meridional $(\beta_v\alpha_v)$ wind speed feedbacks for reanalyses and CMIP5 models described in Table 1. Differences from ERA-Interim are given in parentheses. Differences in bold indicate when a model feedback's 95% confidence interval is outside of the confidence interval for the reanalysis.

No.	$\beta_u\alpha_u$	$\beta_v\alpha_v$
0a	—	—
0b	2.35 ± 1.27	-0.73 ± 0.75
0c	1.87 ± 1.05	-1.54 ± 0.57
1	$\mathbf{0.46 \pm 0.34\ (-1.40)}$	$-1.05 \pm 0.24\ (+0.49)$
2	$1.19 \pm 0.57\ (-0.67)$	$\mathbf{-0.21 \pm 0.20\ (+1.33)}$
3	$2.70 \pm 0.55\ (+0.83)$	$\mathbf{-0.02 \pm 0.29\ (+1.52)}$
4	$1.94 \pm 0.55\ (+0.07)$	$\mathbf{-0.34 \pm 0.33\ (+1.20)}$
5a	$2.02 \pm 0.45\ (+0.15)$	$-0.79 \pm 0.28\ (+0.75)$
5b	$1.47 \pm 0.55\ (-0.39)$	$\mathbf{0.14 \pm 0.35\ (+1.68)}$
6	$2.98 \pm 0.60\ (+1.11)$	$-1.24 \pm 0.53\ (+0.30)$
7a	$1.13 \pm 0.59\ (-0.74)$	$\mathbf{1.53 \pm 0.41\ (+3.07)}$
7b	$0.43 \pm 0.53\ (-1.43)$	$\mathbf{0.92 \pm 0.34\ (+2.46)}$
7c	$2.80 \pm 0.82\ (+0.94)$	$\mathbf{0.16 \pm 0.51\ (+1.70)}$
8a	$2.27 \pm 0.59\ (+0.41)$	$\mathbf{1.59 \pm 0.52\ (+3.13)}$
8b	$\mathbf{4.03 \pm 0.79\ (+2.16)}$	$\mathbf{1.62 \pm 0.46\ (+3.17)}$
9	$3.56 \pm 0.78\ (+1.69)$	$-0.58 \pm 0.38\ (+0.96)$

The meridional WS feedback also varies considerably between models. In this case the feedback varies in sign also, either increasing (positive contribution to LHF damping) or decreasing (negative contribution to LHF damping) the meridional wind speed in response to positive SSTAs. ERA-Interim shows a negative meridional WS feedback. All CMIP5 models have meridional WS feedbacks that are weaker than this, or that are positive. Nine of the 13 CMIP5 models have meridional WS feedbacks significantly different from the ERA-Interim reanalysis (Fig. 9a; Table 3). The meridional WS feedback is linked to the background meridional winds (Fig. 9c), as suggested in the discussion of Fig. 3. Figure 9c uses time-mean area-averaged meridional wind over a region labeled B in Fig. 1 (5°S–5°N, 150°–120°W). This region was chosen as this is the area in Niño-3 where meridional winds show the most bias and variation in the CMIP5 models due to the closer proximity to mean atmospheric circulation biases (i.e., the double ITCZ). Models that have more northerly mean winds in the east Pacific (negative in Fig. 9c) are those that have a more negative meridional WS feedback (correlation of 0.71). The northerly wind anomaly during El Niño increases initial northerly mean winds, increasing evaporation and providing a negative feedback.

As suggested by Fig. 3, the meridional direction of mean winds is related to atmospheric circulation in the equatorial Pacific and can therefore be linked to the double-ITCZ bias (Fig. 9d; correlation of −0.93). This relationship means that the extent of the double-ITCZ bias can be linked to the strength of the meridional WS feedback (Fig. 9e; correlation of −0.63) such that

models with a more extended SE ITCZ tend to have a more negative meridional WS feedback, and therefore a stronger LH damping. Conversely, a less extended SE ITCZ means that the mean winds are more southerly and are therefore weakened by the El Niño northerly wind anomalies, resulting in a positive meridional WS component of LHF damping.

Note here that the observations do not match the interensemble relationships. Similarly, not all the variance in WS feedback is accounted for by the relationship with the mean state. The reanalysis shows less southeast Pacific precipitation than all the CMIP5 models but also a weaker WS feedback and a stronger negative meridional WS component of this feedback. This can be explained by the bias in the model El Niño wind response compared with the observed response (outlined in Fig. 4 and discussion) despite observed mean meridional winds more closely resembling the models with less double-ITCZ bias (e.g., Figs 4a,c). The meridional wind anomaly is consistently too northerly during El Niños and too southerly during La Niñas in CMIP5 models, as shown by the negative Niño-3 meridional wind feedback (dv/dT) in Fig. 9f. Note that in contrast to the meridional WS feedback that uses absolute wind speed anomalies, dv/dT in Fig. 9f uses northerly wind anomalies regressed on SSTAs, so that the sign denotes the direction of anomaly, not just the strength. This is a source of bias for the meridional WS feedback that could result in a more positive feedback, assuming a mean state close to that observed; more northerly wind anomalies during El Niño events cause weakening of mean southerly winds and therefore a weaker LH damping. However, this bias is counteracted in some models by mean state bias.

No significant relationships are found between dv/dT and the double-ITCZ bias. However, it is found that the bias is linked to the atmospheric circulation responses in the CMIP5 models. Models have a tendency to show stronger responses to ENSO events to the south of the equator than observed, resulting in an asymmetry about the equator in the precipitation and meridional wind responses. The asymmetry in precipitation response is shown in Fig. 9f by taking the difference between the South Pacific precipitation feedback (precipitation anomalies averaged over 5°–15°S, 170°–120°W regressed on Niño-3 SSTAs) and North Pacific precipitation feedback (latitude 5°–15°N, same longitude). In ERA-Interim, precipitation response is shown to be somewhat symmetric about the equator (Figs. 4 and 9f). The extent of the CMIP5 precipitation feedback asymmetry is linked to stronger negative dv/dT (correlation of −0.8).

Relationships between LHF damping and other aspects of the mean climate in the equatorial Pacific

(i.e., cold tongue bias) were investigated throughout the course of this study, with few other significant relationships found. A correlation of −0.35 (not significant) is found between Niño-4 mean temperature and LHF damping, as a result of a correlation of −0.3 between the humidity component and mean Niño-4 temperature. There are stronger relationships between mean temperature and the humidity component in a smaller region along the equator in the east Pacific. It is found that mean temperatures along the equator are not significantly related to the double-ITCZ bias. Correlations between the SE ITCZ precipitation measure and mean temperature are −0.08 and 0.40 for Niño-3 and Niño-4 mean temperature, respectively (not shown in figures). This suggests that the two mean state biases should not necessarily relate to ENSO feedbacks in similar ways.

These results confirm then that southeast Pacific precipitation diversity alters meridional winds and can be linked to a diverse meridional WS feedback, and therefore LHF damping. Ultimately, we find that some models in which LHF damping is closer to the observed damping are not necessarily those showing the most accurate mean climates. Some models with a WS feedback closer to observed, such as GFDL CM3, tend to show bias in the mean atmospheric circulation, as well as bias in the El Niño anomalous response. This bias compensation is dependent on the spatial distributions of the mean bias and the anomaly bias within the Niño-3 region in relation to one another. This is something to be aware of when directly comparing Figs. 9d, 9e, and 9f.

c. ENSO atmospheric feedbacks in AMIP runs

As the models with the most biased mean precipitation in the south equatorial Pacific are those with more accurate wind speed feedbacks, this raises a question of the underlying bias of the wind speed feedback. The anomalous winds show consistent errors when compared to observations (Figs. 4 and 9f) and the variation in the mean state seems to alleviate the feedback bias in some models. Feedback bias is examined more closely in atmosphere-only (AMIP) runs of seven of the CMIP5 models used in this study (only seven are selected because of the availability of the relevant output fields). In AMIP simulations, SST is prescribed to the atmosphere model, as opposed to the CMIP5 simulations where an ocean model is coupled to an atmosphere model. This means that SST biases are eliminated, but some atmosphere model bias can still persist.

Figures 10a and 10b show that four of the models show no significant difference in LHF damping in the AMIP runs, compared with the coupled models. Only two models, IPSL-CM5A-LR and IPSL-CM5B-LR, show significant differences in either of the LHF damping

components. Both show significant improvements in LHF damping as a result of a more negative wind speed component. Furthermore, this can be attributed to changes in the zonal WS feedbacks (Figs. 10b,d) as opposed to the meridional WS feedback that was found to dominate the coupled model variation. It is also important to note that the changes shown by components in these models are relatively small.

CMIP LHF feedbacks and AMIP LHF feedbacks are well correlated across the models (see Fig. 10). A weaker correlation (0.56) is shown for the meridional WS feedback. This is perhaps a result of its link to mean state biases in the coupled runs that are reduced for some models in AMIP runs. Nonetheless, four of the seven AMIP models studied showed no significant difference in meridional WS feedback between CMIP and AMIP runs. It is also found that the asymmetries about the equator in precipitation response and meridional wind response during ENSO events persist in AMIP runs, and there is once again a correlation between the two (Fig. 10e).

AMIP results find that a number of errors that drive variation in the LHF damping persist in the atmosphere model. We note that the relationship with southeast Pacific precipitation does not exist for the AMIP models, despite mean precipitation biases still being present, albeit at a much weaker amplitude. However, the variation in mean precipitation is somewhat reduced in AMIP, as is the number of models used in the study, so drawing a robust conclusion from this is difficult.

6. Conclusions and discussion

This study aims to identify relationships between the common double-ITCZ bias and ENSO atmospheric feedbacks, with a particular focus on damping by evaporative heat flux. We implement an ENSO feedback decomposition to identify underlying mechanisms of feedback bias and diversity.

Significant biases are found in the mean state equatorial Pacific climate. Almost all models show the cold tongue and double-ITCZ bias to some extent, in agreement with other CMIP5 studies (Brown et al. 2013; Bellenger et al. 2014; Zhang et al. 2015; Adam et al. 2016). SSTs along the equator in the Pacific tend to be too cool. Similarly, precipitation and atmospheric ascent is too weak along the equator compared with reanalysis data. Biases are also found to the north and south of the equator. Precipitation tends to be too strong in the northwest and southeast Pacific. In particular, the zonal extent of the South Pacific precipitation band (SE ITCZ) shows diversity between the CMIP5 models. These mean state atmospheric circulation biases and diversity impact the mean state and El Niño–induced
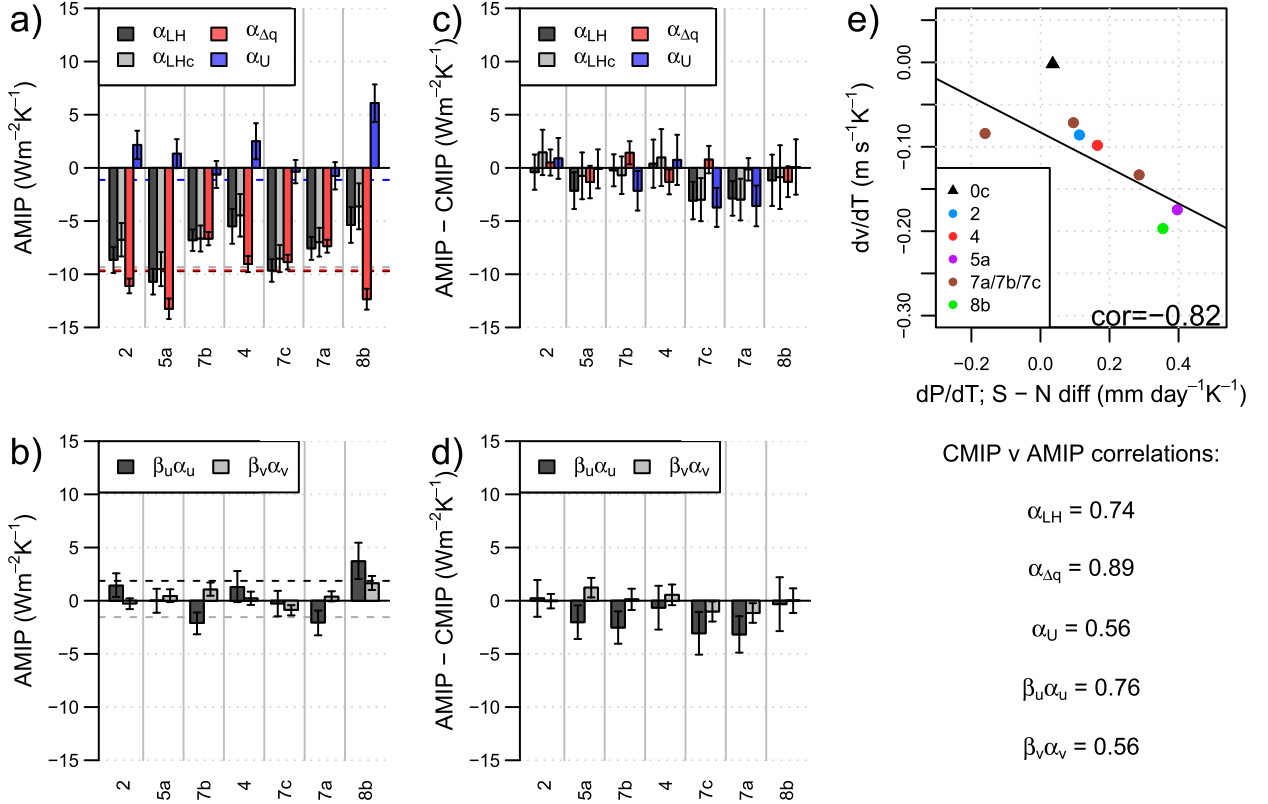
FIG. 10. (a) AMIP Niño-3 latent heat damping calculated using the latent heat flux field given by the model (α_{LH}; dark gray bars), latent heat damping calculated using latent heat flux reconstructed using bulk formula (α_{LHc}; light gray bars), humidity anomaly component of α_{LH} ($\alpha_{\Delta q}$, red bars), and the wind speed anomaly component of α_{LH} (α_U, blue bars). (b) AMIP zonal wind speed feedback ($\beta_u\alpha_u$, dark gray bars) and meridional wind speed feedback ($\beta_v\alpha_v$, light gray bars). (c),(d) As in (a),(b), but for AMIP feedback minus CMIP feedback. (e) As in Fig. 9f, but for AMIP runs. Error bars show the 95% confidence interval from the linear fit of the feedbacks. Horizontal dashed lines show the OAFlux values in (a) and the ERA-Interim values in (b).

winds along the equator, resulting in differences in ENSO atmospheric feedbacks between the models.

Latent heat flux damping is somewhat diversely represented and tends to be too weak in these CMIP5 models, in agreement with Bellenger et al. (2014). In general, like in the CMIP3 models (Lloyd et al. 2012), it is found that the LHF damping bias can be the result of a combination of biases in both the dominant humidity gradient feedback and the weaker wind speed (WS) feedback. However, the majority of CMIP5 models used in this study show a relatively strong positive WS feedback contribution to LHF damping compared with the reanalyses, which tend to show a small WS feedback. The interensemble variation of LHF damping is also primarily governed by the WS feedback diversity. This is in spite of humidity gradient anomalies being the dominant driver of east Pacific LHF, in keeping with other studies (Alexander and Scott 1997; Lloyd et al. 2012).

There are two areas of focus for wind speed feedback diversity; the first is the CMIP5 bias in relation to observations and the second is the interensemble diversity.

The proposed mechanisms behind these differences are slightly different from one another. CMIP5 models have a tendency toward a larger positive contribution to LHF damping by the wind speed feedback. This can be attributed to the different anomalous responses of the models compared to the reanalyses. The observed El Niño response shows an eastward shift in the ascending branch of the Walker circulation, a southward ITCZ shift and a northeastward South Pacific precipitation shift (see Fig. 4). These responses induce northerly wind speed anomalies north of the equator and southerly anomalies south of the equator, weakening and increasing the initial winds respectively. This contrast results in a weak area-averaged Niño-3 wind speed component of the LHF feedback, although an overall strengthening of the (southeasterly) winds along the equator is shown in ERA-Interim during El Niño. However, the CMIP5 models El Niño responses are mainly dominated by an eastward extension of the already overly extended SE ITCZ, inducing northerly anomalies (Fig. 9f). Initial mean southeasterly winds

would be consequently reduced during El Niño, resulting in a generally more positive WS feedback, reducing LHF damping.

For the second focus, the diversity of wind speed feedback between CMIP5 models, it is found that as well as the errors in the anomalous wind direction, there is also variation in the mean meridional wind direction depending on the zonal extent of the SE ITCZ that can explain some of the WS feedback variance. A more extended SE ITCZ can result in northeasterly winds to the south of the equator, which are then increased by the El Niño–induced northerly anomalies, shown in Fig. 4, thus causing a more negative meridional wind speed feedback and increasing LHF damping of SST. Conversely, a less extended SE ITCZ means that the mean southeasterly winds are reduced during El Niño. This creates a more positive meridional wind speed feedback and therefore a weaker LHF damping. Ultimately, we can conclude that models that simulate WS and LHF feedbacks closer to observed may not be doing so for the correct reasons; that is, the weaker WS feedbacks, and hence stronger LHF dampings, may be a product of errors in both the mean state and anomalous response. It is difficult to state from this study what the implications might be for LHF damping if the mean state errors were corrected. There exists an underlying bias in the anomalous meridional winds during events. This has been linked to a spatial asymmetry in the equatorial Pacific precipitation response in both CMIP5 and AMIP runs. It is possible this bias may change should the mean state be changed, or it may persist if these errors lie in the underlying dynamics of the model. However, the results highlight areas that are important to consider when aiming to correct coupled model errors.

This study highlights the importance of the meridional wind speed feedback in damping ENSO, something that has been largely overlooked in CMIP3 latent heat flux damping studies (e.g., Lin 2007; Lloyd et al. 2011). Links between the mean atmospheric circulation and key ENSO atmospheric feedbacks are established here with the use of feedback decomposition. There also exists a strong relationship in a subset of these models between LHF damping and ENSO amplitude (correlation of −0.75; not shown in figures) as a result of a strong relationship between the wind speed feedback and ENSO amplitude (correlation of −0.63). This result depends on the exclusion of MIROC5. MIROC5 is shown in Fig. 6 to have a significantly nonlinear wind speed feedback, resulting in this model being an outlier in these relationships. Note that this relationship with ENSO amplitude exists for all models in this study if examining LHF damping during El Niño events only. This demonstrates the importance of interensemble variation of these feedbacks in relation to ENSO event strength.

This study focuses on atmospheric responses relevant to ENSO LHF damping. Note that the surface zonal winds also interact with the ocean, resulting in further feedbacks on SSTA. For example, in the east equatorial Pacific surface zonal winds impact subsurface ocean upwelling and therefore SSTA. This means that ocean feedbacks may also affect latent heat flux. Here, ocean interactions on LHF damping are considered as second-order terms that are negligible throughout this analysis and so focus on only atmosphere responses.

Analysis of atmosphere-only (AMIP) models reveals that biases in LHF feedbacks still persist even when SSTs are prescribed. These results suggest that the atmosphere model may play an important role in determining the LHF damping bias. This raises the possibility that both the double-ITCZ bias and the ENSO LHF feedback bias have an origin in the atmosphere models and that improvements in both the mean tropical Pacific precipitation and ENSO physics in coupled models may be accelerated by focusing on correcting errors in the atmosphere component. However, the number of AMIP models that were available for study was very limited due to data availability, so it is difficult to draw strong conclusions from this.

Results found here can be used to prioritize the development of future climate models to improve our confidence in ENSO projections. This work can also be used to assess drifts in seasonal forecast systems and their impact on seasonal ENSO predictions. Additionally, ENSO feedback diversity identified here may also have implications for diversity in modeled ENSO teleconnections (e.g., Kim et al. 2017), providing a basis for further work in this area.

Climate Model Diagnosis and Intercomparison provides coordinating support and led development of software infrastructure in partnership with the Global Organization for Earth System Science Portals.

REFERENCES

AchutaRao, K., and K. R. Sperber, 2006: ENSO simulation in coupled ocean–atmosphere models: Are the current models better? *Climate Dyn.*, **27**, 1–15, doi:10.1007/s00382-006-0119-7.

Adam, O., T. Schneider, F. Brient, and T. Bischoff, 2016: Relation of the double-ITCZ bias to the atmospheric energy budget in climate models. *Geophys. Res. Lett.*, **43**, 7670–7677, doi:10.1002/2016GL069465.

Adler, R. F., and Coauthors, 2003: The version-2 Global Precipitation Climatology Project (GPCP) monthly precipitation analysis (1979–present). *J. Hydrometeor.*, **4**, 1147–1167, doi:10.1175/1525-7541(2003)004<1147:TVGPCP>2.0.CO;2.

Alexander, M. A., and J. D. Scott, 1997: Surface flux variability over the North Pacific and North Atlantic Oceans. *J. Climate*, **10**, 2963–2978, doi:10.1175/1520-0442(1997)010<2963:SFVOTN>2.0.CO;2.

Ambaum, M. H. P., 2010: *Thermal Physics of the Atmosphere.* Wiley-Blackwell, 256 pp.

An, S.-L., and F.-F. Jin, 2000: An eigen analysis of the interdecadal changes in the structure and frequency of ENSO mode. *Geophys. Res. Lett.*, **27**, 2573–2576, doi:10.1029/1999GL011090.

Bellenger, H., E. Guilyardi, J. Leloup, M. Lengaigne, and J. Vialard, 2014: ENSO representation in climate models: From CMIP3 to CMIP5. *Climate Dyn.*, **42**, 1999–2018, doi:10.1007/s00382-013-1783-z.

Bony, S., K.-M. Lau, and Y. C. Sud, 1997: Sea surface temperature and large-scale circulation influences on tropical greenhouse effect and cloud radiative forcing. *J. Climate*, **10**, 2055–2077, doi:10.1175/1520-0442(1997)010<2055:SSTALS>2.0.CO;2.

Brown, J. R., A. F. Moise, and R. A. Colman, 2013: The South Pacific convergence zone in CMIP5 simulations of historical and future climate. *Climate Dyn.*, **41**, 2179–2197, doi:10.1007/s00382-012-1591-x.

Brunke, M. A., X. Zeng, and S. Anderson, 2002: Uncertainties in sea surface turbulent flux algorithms and data sets. *J. Geophys. Res.*, **107**, 3141, doi:10.1029/2001JC000992.

Capotondi, A., A. Wittenberg, and S. Masina, 2006: Spatial and temporal structure of tropical Pacific interannual variability in 20th century coupled simulations. *Ocean Modell.*, **15**, 274–298, doi:10.1016/j.ocemod.2006.02.004.

Chang, P., and S. G. Philander, 1994: A coupled ocean–atmosphere instability of relevance to the seasonal cycle. *J. Atmos. Sci.*, **51**, 3627–3648, doi:10.1175/1520-0469(1994)051<3627:ACOIOR>2.0.CO;2.

Chikira, M., and M. Sugiyama, 2010: A cumulus parameterization with state-dependent entrainment rate. Part I: Description and sensitivity to temperature and humidity profiles. *J. Atmos. Sci.*, **67**, 2171–2193, doi:10.1175/2010JAS3316.1.

Choi, K., G. Vecchi, and A. Wittenberg, 2013: ENSO transition, duration, and amplitude asymmetries: Role of the nonlinear wind stress coupling in a conceptual model. *J. Climate*, **26**, 9462–9476, doi:10.1175/JCLI-D-13-00045.1.

Dee, D. P., and Coauthors, 2011: The ERA-Interim reanalysis: Configuration and performance of the data assimilation system. *Quart. J. Roy. Meteor. Soc.*, **137**, 553–597, doi:10.1002/qj.828.

de Szoeke, S. P., and S. Xie, 2008: The tropical eastern Pacific seasonal cycle: Assessment of errors and mechanisms in IPCC AR4 coupled ocean–atmosphere general circulation models. *J. Climate*, **21**, 2573–2590, doi:10.1175/2007JCLI1975.1.

Dommenget, D., T. Bayr, and C. Frauen, 2013: Analysis of the nonlinearity in the pattern and time evolution of El Niño southern oscillation. *Climate Dyn.*, **40**, 2825–2847, doi:10.1007/s00382-012-1475-0.

Fairall, C. W., E. F. Bradley, D. P. Rogers, J. B. Edson, and G. S. Young, 1996: Bulk parameterization of air–sea fluxes for Tropical Ocean–Global Atmosphere Coupled Ocean–Atmosphere Response Experiment. *J. Geophys. Res.*, **101**, 3747–3764, doi:10.1029/95JC03205.

——, ——, J. E. Hare, A. A. Grachev, and J. B. Edson, 2003: Bulk parameterization of air–sea fluxes: Updates and verification for the COARE algorithm. *J. Climate*, **16**, 571–591, doi:10.1175/1520-0442(2003)016<0571:BPOASF>2.0.CO;2.

Fedorov, A. V., and S. G. Philander, 2001: A stability analysis of tropical ocean–atmosphere interactions: Bridging measurements and theory for El Niño. *J. Climate*, **14**, 3086–3101, doi:10.1175/1520-0442(2001)014<3086:ASAOTO>2.0.CO;2.

Ferrett, S., and M. Collins, 2016: ENSO feedbacks and their relationships with the mean state in a flux adjusted ensemble. *Climate Dyn.*, doi:10.1007/s00382-016-3270-9, in press.

Frey, H., M. Latif, and T. Stockdale, 1997: The coupled GCM ECHO-2. Part I: The tropical Pacific. *Mon. Wea. Rev.*, **125**, 703–720, doi:10.1175/1520-0493(1997)125<0703:TCGEPI>2.0.CO;2.

Goff, J. A., 1957: Saturation pressure of water on the new Kelvin temperature scale. *Trans. Amer. Soc. Heat. Vent. Eng.*, **63**, 347–354.

——, and S. Gratch, 1946: Low-pressure properties of water from −160 to 212°F. *Trans. Amer. Soc. Heat. Vent. Eng.*, **52**, 95–122.

Guilyardi, E., 2006: El Niño–mean state–seasonal cycle interactions in a multi-model ensemble. *Climate Dyn.*, **26**, 329–348, doi:10.1007/s00382-005-0084-6.

Hess, P. G., D. S. Battisti, and P. J. Rasch, 1993: Maintenance of the intertropical convergence zones and the large-scale tropical circulation on a water-covered Earth. *J. Atmos. Sci.*, **50**, 691–713, doi:10.1175/1520-0469(1993)050<0691:MOTICZ>2.0.CO;2.

Jin, F.-F., S. T. Kim, and L. Bejarano, 2006: A coupled-stability index of ENSO. *Geophys. Res. Lett.*, **33**, L23708, doi:10.1029/2006GL027221.

Kanamitsu, M., W. Ebisuzaki, J. Woollen, S.-K. Yang, J. Hnilo, M. Fiorino, and G. Potter, 2002: NCEP–DOE AMIP-II Reanalysis (R-2). *Bull. Amer. Meteor. Soc.*, **83**, 1631–1643, doi:10.1175/BAMS-83-11-1631.

Kim, S., H.-Y. Son, and J.-S. Kug, 2017: How well do climate models simulate atmospheric teleconnections over the North Pacific and East Asia associated with ENSO. *Climate Dyn.*, **48**, 971–985, doi:10.1007/s00382-016-3121-8.

Kim, S. T., and F.-F. Jin, 2011: An ENSO stability analysis. Part II: Results from the twentieth and twenty-first century simulations of the CMIP3 models. *Climate Dyn.*, **36**, 1609–1627, doi:10.1007/s00382-010-0872-5.

——, W. Cai, F.-F. Jin, A. Santoso, L. Wu, E. Guilyardi, and S.-I. An, 2014a: Response of El Niño sea surface temperature variability to greenhouse warming. *Nat. Climate Change*, **4**, 786–790, doi:10.1038/nclimate2326.

——, ——, ——, and J.-Y. Yu, 2014b: ENSO stability in coupled climate models and its association with mean state. *Climate Dyn.*, **42**, 3313–3321, doi:10.1007/s00382-013-1833-6.

Kubota, M., N. Iwabe, M. Cronin, and H. Tomita, 2008: Surface heat fluxes from the NCEP/NCAR and NCEP/DOE reanalyses at the Kuroshio Extension Observatory buoy site. *J. Geophys. Res.*, **113**, C02009, doi:10.1029/2007JC004338.

Li, G., and S. Xie, 2012: Origins of tropical-wide SST biases in CMIP multi-model ensembles. *Geophys. Res. Lett.*, **39**, L22703, doi:10.1029/2012GL053777.

——, and ——, 2014: Tropical biases in CMIP5 multimodel ensemble: The excessive equatorial Pacific cold tongue and double ITCZ problems. *J. Climate*, **27**, 1765–1780, doi:10.1175/JCLI-D-13-00337.1.

Li, T., and S. Philander, 1996: On the annual cycle of the eastern equatorial Pacific. *J. Climate*, **9**, 2986–2998, doi:10.1175/1520-0442(1996)009<2986:OTACOT>2.0.CO;2.

Lin, J., 2007: The double-ITCZ problem in IPCC AR4 coupled GCMs: Ocean–atmosphere feedback analysis. *J. Climate*, **20**, 4497–4525, doi:10.1175/JCLI4272.1.

Lloyd, J., E. Guilyardi, H. Weller, and J. Slingo, 2009: The role of atmosphere feedbacks during ENSO in the CMIP3 models. *Atmos. Sci. Lett.*, **10**, 170–176, doi:10.1002/asl.227.

——, ——, and ——, 2011: The role of atmosphere feedbacks during ENSO in the CMIP3 models. Part II: Using AMIP runs to understand the heat flux feedback mechanisms. *Climate Dyn.*, **37**, 1271–1292, doi:10.1007/s00382-010-0895-y.

——, ——, and ——, 2012: The role of atmosphere feedbacks during ENSO in the CMIP3 models. Part III: The shortwave flux feedback. *J. Climate*, **25**, 4275–4293, doi:10.1175/JCLI-D-11-00178.1.

Luo, J., S. Masson, E. Roeckner, G. Madec, and T. Yamagata, 2005: Reducing climatology bias in an ocean–atmosphere CGCM with improved coupling physics. *J. Climate*, **18**, 2344–2360, doi:10.1175/JCLI3404.1.

Mechoso, C. A., and Coauthors, 1995: The seasonal cycle over the tropical Pacific in coupled ocean–atmosphere general circulation models. *Mon. Wea. Rev.*, **123**, 2825–2838, doi:10.1175/1520-0493(1995)123<2825:TSCOTT>2.0.CO;2.

Mitchell, T., and J. Wallace, 1992: The annual cycle in equatorial convection and sea surface temperature. *J. Climate*, **5**, 1140–1156, doi:10.1175/1520-0442(1992)005<1140:TACIEC>2.0.CO;2.

Moore, G. W. K., and I. A. Renfrew, 2002: An assessment of the surface turbulent heat fluxes from the NCEP–NCAR reanalysis over the western boundary currents. *J. Climate*, **15**, 2020–2037, doi:10.1175/1520-0442(2002)015<2020:AAOTST>2.0.CO;2.

Philander, S., D. Gu, G. Lambert, T. Li, D. Halpern, N. Lau, and R. C. Pacanowski, 1996: Why the ITCZ is mostly north of the equator. *J. Climate*, **9**, 2958–2972, doi:10.1175/1520-0442(1996)009<2958:WTIIMN>2.0.CO;2.

Philip, S., and G. J. van Oldenborgh, 2009: Significant atmospheric nonlinearities in the ENSO cycle. *J. Climate*, **22**, 4014–4028, doi:10.1175/2009JCLI2716.1.

Renfrew, I. A., G. W. K. Moore, P. Guest, and K. Bumke, 2002: A comparison of surface layer and surface turbulent flux observations over the Labrador Sea with ECMWF analyses and NCEP reanalyses. *J. Phys. Oceanogr.*, **32**, 383–400, doi:10.1175/1520-0485(2002)032<0383:ACOSLA>2.0.CO;2.

Santoso, A., W. Cai, M. H. England, and S. J. Phipps, 2011: The role of the Indonesian Throughflow on ENSO dynamics in a coupled climate model. *J. Climate*, **24**, 585–601, doi:10.1175/2010JCLI3745.1.

——, S. McGregor, F.-F. Jin, W. Cai, M. England, S.-I. An, M. McPhaden, and E. Guilyardi, 2013: Late-twentieth-century emergence of the El Niño propagation asymmetry and future projections. *Nature*, **504**, 126–130, doi:10.1038/nature12683.

Schiffer, R. A., and W. B. Rossow, 1983: The International Satellite Cloud Climatology Project (ISCCP): The first project of the World Climate Research Programme. *Bull. Amer. Meteor. Soc.*, **64**, 779–784.

Schneider, E. K., 2002: Understanding differences between the equatorial Pacific as simulated by two coupled GCMs. *J. Climate*, **15**, 449–469, doi:10.1175/1520-0442(2002)015<0449:UDBTEP>2.0.CO;2.

Song, X., and G. J. Zhang, 2009: Convection parameterization, tropical Pacific double ITCZ, and upper-ocean biases in the NCAR CCSM3. Part I: Climatology and atmospheric feedback. *J. Climate*, **22**, 4299–4315, doi:10.1175/2009JCLI2642.1.

Taylor, K. E., R. J. Stouffer, and G. A. Meehl, 2012: An overview of CMIP5 and the experiment design. *Bull. Amer. Meteor. Soc.*, **93**, 485–498, doi:10.1175/BAMS-D-11-00094.1.

Vannière, B., E. Guilyardi, G. Madec, F. Doblas-Reyes, and S. Woolnough, 2013: Using seasonal hindcasts to understand the origin of the equatorial cold tongue bias in CGCMs and its impact on ENSO. *Climate Dyn.*, **40**, 963–981, doi:10.1007/s00382-012-1429-6.

Wallace, J. M., 1992: Effect of deep convection on the regulation of tropical sea surface temperature. *Nature*, **357**, 230–231, doi:10.1038/357230a0.

Xie, S.-P., and S. G. H. Philander, 1994: A coupled ocean–atmosphere model of relevance to the ITCZ in the eastern Pacific. *Tellus*, **46A**, 340–350, doi:10.3402/tellusa.v46i4.15484.

Yu, L., and R. A. Weller, 2007: Objectively analyzed air–sea heat fluxes for the global ice-free oceans (1981–2005). *Bull. Amer. Meteor. Soc.*, **88**, 527–539, doi:10.1175/BAMS-88-4-527.

Zhang, G. J., and M. J. McPhaden, 1995: The relationship between sea surface temperature and latent heat flux in the equatorial Pacific. *J. Climate*, **8**, 589–605, doi:10.1175/1520-0442(1995)008<0589:TRBSST>2.0.CO;2.

——, and H. Wang, 2006: Toward mitigating the double ITCZ problem in NCAR CCSM3. *Geophys. Res. Lett.*, **33**, L06709, doi:10.1029/2005GL025229.

——, and X. Song, 2010: Convection parameterization, tropical Pacific double ITCZ, and upper-ocean biases in the NCAR CCSM3. Part II: Coupled feedback and the role of ocean heat transport. *J. Climate*, **23**, 800–812, doi:10.1175/2009JCLI3109.1.

Zhang, T., and D. Sun, 2014: ENSO asymmetry in CMIP5 models. *J. Climate*, **27**, 4070–4093, doi:10.1175/JCLI-D-13-00454.1.

Zhang, W., and F.-F. Jin, 2012: Improvements in the CMIP5 simulations of ENSO-SSTA meridional width. *Geophys. Res. Lett.*, **39**, L23704, doi:10.1029/2012GL053588.

——, ——, J. Zhao, and J. Li, 2013: On the bias in simulated ENSO SSTA meridional widths of CMIP3 models. *J. Climate*, **26**, 3173–3186, doi:10.1175/JCLI-D-12-00347.1.

Zhang, X., H. Liu, and M. Zhang, 2015: Double ITCZ in coupled ocean–atmosphere models: From CMIP3 to CMIP5. *Geophys. Res. Lett.*, **42**, 8651–8659, doi:10.1002/2015GL065973.